Lithos 114 (2010) 423–436

Contents lists available at ScienceDirect

Lithos

journal homepage: www.elsevier.com/locate/lithos

Zircon U–Pb age and Sr–Nd–Hf isotope geochemistry of Permian granodiorite and associated gabbro in the Songliao Block, NE China and implications for growth of juvenile crust

Shen Liu [a,b,d,*], Ruizhong Hu [a], Shan Gao [b], Caixia Feng [b,d], Guangying Feng [b], Ian M. Coulson [d], Cai Li [c], Tao Wang [b], Youqiang Qi [b]

[a] State Key Laboratory of Ore Deposit Geochemistry, Institute of Geochemistry, Chinese Academy of Sciences, Guiyang 550002, China
[b] State Key Laboratory of Geological Processes and Mineral Resources, China University of Geosciences, Wuhan 430074, China
[c] College of Earth Sciences, Jilin University, Changchun 130061, China
[d] Solid Earth Studies Laboratory, Department of Geology, University of Regina, Regina, Saskatchewan, Canada S4S 0A2

ARTICLE INFO

Article history:
Received 20 June 2009
Accepted 9 October 2009
Available online 21 October 2009

Keywords:
Post-orogenic
Late Palaeozoic magmatism
Granodiorite
Gabbro
Lithospheric delamination
Crustal growth
NE China

ABSTRACT

Post-orogenic granitic and associated mafic rocks from northeastern (NE) China consist of granodiorite and gabbro intrusions. We report here upon new U–Pb zircon ages, geochemical data and Sr–Nd–Hf isotopic data for these rocks. LA-ICP-MS U–Pb zircon analysis yields an age of 262.8 ± 1.0 Ma for the granitic rocks, and a uniform age of 262.1 ± 0.7 Ma for the gabbro. Most of the granitic and mafic rocks are characterised by low $K_2O + Na_2O$, and pertain to the subalkaline series in the total alkali–silica diagram. The granodiorite samples show low $(^{87}Sr/^{86}Sr)_i$ ranging from 0.700 to 0.705, positive $\varepsilon_{Nd}(t)$ values from +0.3 to +0.8, and large variation in $\varepsilon_{Hf}(t)$ values of between −4.0 and +2.5, indicating that both newly underplated basalt (70–80%) and ancient lower crustal sources (20–30%) contributed to their origin. Furthermore, positive $\varepsilon_{Hf}(t)$ values with two-stage model ages (T_{DM2}) of 1123–1260 Ma, together with Nd model ages (960–1000 Ma), suggest an important episode of crustal growth during the Meso-Neoproterozoic beneath the Songliao Block. In contrast, the investigated gabbro is characterised by relatively high $(^{87}Sr/^{86}Sr)_i$ ratios (0.707–0.708), negative $\varepsilon_{Nd}(t)$ (−5.9 to −5.3) and $\varepsilon_{Hf}(t)$ values (−5.0 to −2.3), implying that this was derived from an enriched mantle source. The geochemical data indicate that the granitic magmas underwent separation of clinopyroxene, hornblende, K-feldspar, plagioclase, Ti-bearing phases (e.g., rutile, ilmenite, titanite), apatite and zircon during their evolution. Whereas the gabbro is characterised by low MgO (2.92–3.92 wt.%), Mg# (35–41) and compatible elements content, such as Cr (10–68 ppm), Co (16–31 ppm) and Ni (5.7–33 ppm), features of a more evolved mafic magma. There is no evidence that the granitic and mafic rocks were affected by crustal contamination during emplacement. Our interpretation is that the two coeval intrusive suites were both formed in a post-orogenic extensional setting, related to lithospheric delamination or 'collapse' of the Central Asian Orogenic Belt (CAOB) (Xingmeng orogenic Belt in China).

1. Introduction

Phanerozoic granites are widespread (~3×10^5 km^2, Wu et al., 2007a) throughout northeastern China (NE China). Recent studies indicate that many of these granites contain a large proportion of juvenile crustal material, thus suggesting that the Phanerozoic was an extensive period of crustal growth for this part of the world (Wu et al., 2000a; Chen et al., 2000; Zhao et al., 2000; Jahn et al., 2000a,b; Wu et al., 2001, 2002; Chen and Jahn, 2002; Jahn, 2002; Wu et al., 2003a,b; Cheng et al., 2006; Ge et al., 2007; Wu et al., 2007a). It is precisely because of the special significance of this part of Asia to models of global crustal growth that systematic isotopic and petrogenetic studies of all of the Phanerozoic granitic intrusions in NE China is needed.

NE China is generally regarded to form part of the Hercynian Fold belt; as such, most of the granites present in NE China were traditionally considered to be of Late Palaeozoic (or Hercynian) age (Wu et al., 2000a). Recent investigations, however, have indicated that in fact these intrusions were mainly formed during the early Mesozoic (Wu et al., 2000a, 2007a), and further, that 'true' Late Palaeozoic granitoid rocks are rare, being distributed only in the Jiamusi Block in the east and in the Great Xing'an Range in the west (Fig. 1a) (Wu et al., 2000b, 2001, 2002). In the Songliao Block (Fig. 1a), Late Palaeozoic granites have not yet been recorded. Accordingly, in order to further understand the spatio–temporal relationships of the voluminous granitic rocks in NE China, precise geochronological and geochemical data are required.

* Corresponding author. State Key Laboratory of Ore Deposit Geochemistry, Institute of Geochemistry, Chinese Academy of Sciences, Guiyang 550002, China. Tel.: +86 851 5895187; fax: +86 851 5891664.
E-mail address: liushen@vip.gyig.ac.cn (S. Liu).

0024-4937/$ – see front matter
doi:10.1016/j.lithos.2009.10.009

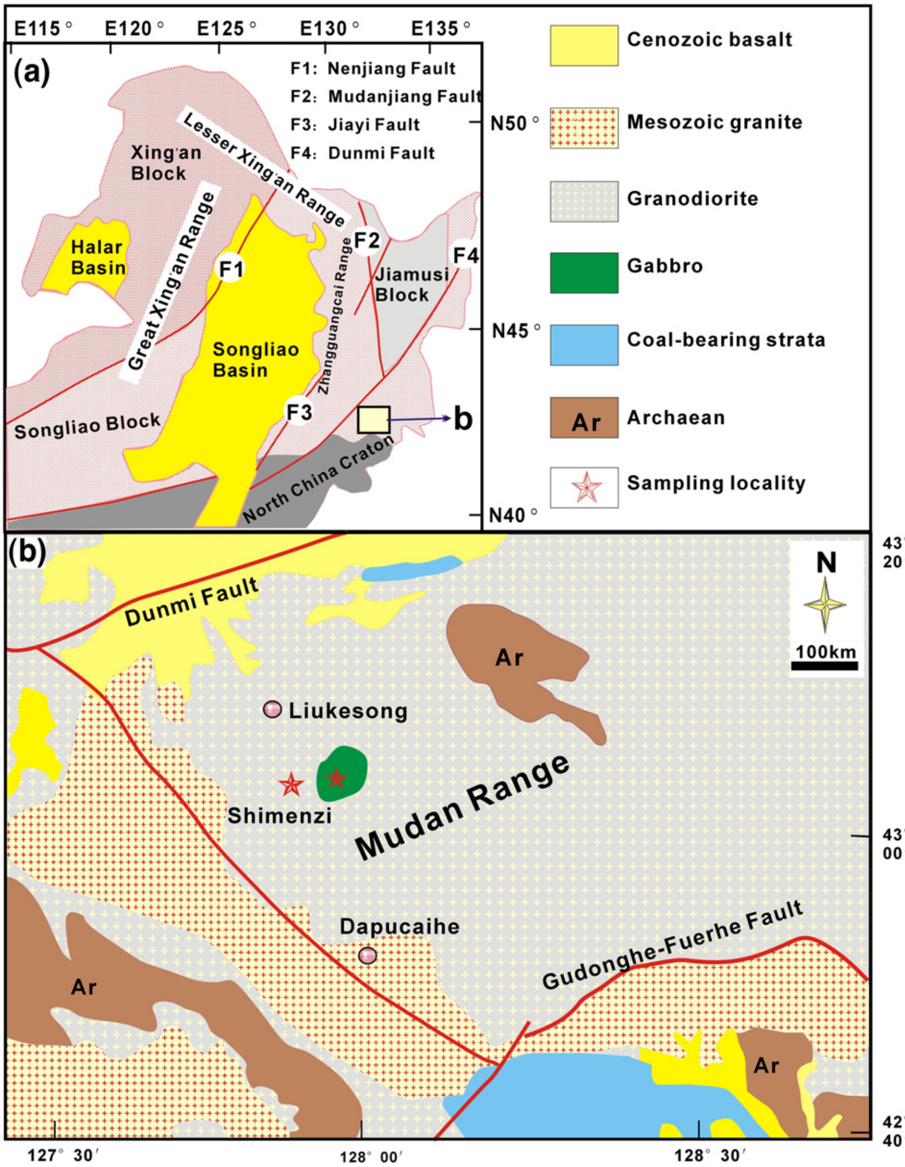

Fig. 1. (a) Tectonic divisions of NE China (cited from Wu et al., 2002). (b) Geological map of the study area that includes the sampling localities for the granodiorite and gabbro samples.

For a long time, the existence of Late Palaeozoic, mafic magmatism in the east of the Jilin and Heilongjiang provinces has proven controversial. For example, the mafic–ultramafic intrusions distributed at Hongqiling and Piaohechuan (Cu–Ni deposits), in the east of the Jilin Province, had been considered to have been emplaced during the Late Palaeozoic (Qin, 1995); more precise geochronology, however, now suggests that they are the results of Indosinian magmatism (Wu et al., 2004a). Although, some researchers have documented, recently, the presence of Late Palaeozoic mafic magmatic activity in the area of Yanbian, eastern Jilin Province in the Chinese literature (e.g., Sun et al., 2008; Zhao et al., 2008), the source features and petrogenesis of these mafic rocks have not yet been regarded.

Accordingly, this study provides good opportunity to further document the ages, and the chemical and isotopic characteristics of Late Palaeozoic granodiorite and associated gabbro in NE China; herein we undertake a systematic isotopic and geochemical investigation of representative intrusions from the Songliao Block. Moreover, in this paper, we report new ages and Sr–Nd–Hf isotopic data to constrain their petrogenesis and use this data to discuss their implications for crustal growth in NE China during the Phanerozoic.

2. Geological setting and petrology

NE China is divided by the Nenjiang (F1) and Mudanjiang (F2) Faults (Fig. 1a) into three microcontinental blocks (i.e., the Jiamusi Block in the east, Songliao Block in the centre and Xing'an Block in the northwest) (Ye et al., 1994). The Jiamusi Block is mainly composed of two sequences of Precambrian metamorphic rocks: the Mashan and Heilongjiang Groups (Wu et al., 2003a,b). The Mashan Group, that has been metamorphosed at granulite facies conditions (Wilde et al., 2000), comprises granulite, marble, graphitic schist, together with gneiss and garnet-bearing granite. By contrast, the Heilongjiang Group, exposed along the Mudanjiang Fault (F2) between the Jiamusi and Songliao Blocks (Fig.1a), is characterised by highly deformed blueschist facies rocks, including glaucophane schist, marble and chert (Wu et al., 2003a,b). The Songliao Block consists of the Lesser Xing'an Range in the north, the Songliao sedimentary basin in the centre and the Zhangguangcai Range in the east (Fig. 1a). Voluminous Phanerozoic granitic rocks are widespread throughout the Block, intruding both mountainous regions (JBGMR, 1988; IMBGMR, 1990; HBGMR, 1993) and beneath the Songliao basins (Wu et al., 2001).

Furthermore, Proterozoic metamorphic rocks with banded iron formation (Dongfengshan Group) occur within the eastern Lesser Xing'an and northern Zhangguangcai Ranges (HBGMR, 1993; Wu et al., 2003a, b). The Xing'an Block is located within the Great Xing'an Range (Fig. 1a) where extensive Mesozoic volcanic and granitic rocks, as well as Proterozoic metamorphic rocks and Palaeozoic strata are exposed (HBGMR, 1993; Wu et al., 2003a, b).

Available age constraints suggest that the Phanerozoic granitic rocks in NE China were mainly formed during the Mesozoic, ranging from 230 to 120 Ma (Wu et al., 2000a,b; Zhang et al., 2002a,b; Wu et al., 2002; Wu et al., 2003a,b, 2004b; Guo et al., 2004a; Yang et al., 2004; Zhang et al., 2004; Sun et al., 2005; Wu et al., 2005; Ge et al., 2005; Cheng et al., 2006; Zhang et al., 2006; Wu et al., 2007a; Ge et al., 2007; Wu et al., 2008). Minor Palaeozoic granitic magmatism is mainly distributed in the Great Xing'an Range and the Jiamusi Block (HBGMR, 1993; Wu et al., 2000b, 2001, 2002; Ge et al., 2007). At present, examples of Palaeozoic granitic rocks are lacking in the Songliao Block. In contrast to the voluminous granitic magmatism that is present in NE China, there are few reported occurrences of Phanerozoic mafic intrusions (JBGMR, 1988; IMBGMR, 1990; HBGMR, 1993).

The study area for our samples is located within the Songliao Block, south of the Dunmi Fault (Fig. 1a and b). Here granodiorite outcrops as a large batholith intruding Archaean strata, which was in turn intruded by Cenozoic mafic rocks, Mesozoic granitoids, and a small mafic intrusion of gabbro that is also the focus of this study (Fig. 1b). The studied granitic and mafic rocks are neither deformed nor metamorphosed.

The granodiorite consists of plagioclase (0.6–3.0 mm, 45–55%), K-feldspar (0.5–2.5 mm, 10–15%), quartz (0.5–2.5 mm, 20–25%), biotite (0.5–2.0 mm, 10–15%) and minor hornblende (3–5%). Accessory phases include magnetite, titanite, apatite and zircon. The gabbro is intermediate-coarse grained and porphyritic, comprising phenocrysts of interstitial, anhedral or subhedral clinopyroxene (3.0–6.0 mm,13–14%), plagioclase

Table 1
LA-ICP-MS U–Pb isotopic data for the zircons from the studied granodiorites (SMZG-01) and gabbros (SMZM-01).

SMZG-01	Isotopic ratios										Age (Ma)					
Spot	Th (ppm)	U (ppm)	Pb (ppm)	Th/U	$^{207}Pb/^{206}Pb$	1 s	$^{207}Pb/^{235}U$	1 s	$^{206}Pb/^{238}U$	1 s	$^{207}Pb/^{206}Pb$	1 s	$^{207}Pb/^{235}U$	1 s	$^{206}Pb/^{238}U$	1 s
1	206	330	17.6	0.62	0.0536	0.0016	0.2973	0.0086	0.0413	0.0004	356	49	264	7	261	2
2	129	234	12.6	0.55	0.0533	0.0021	0.3005	0.0115	0.0411	0.0004	341	68	267	9	260	3
3	87.6	260	13.1	0.34	0.0523	0.0017	0.2989	0.0093	0.0417	0.0004	299	54	266	7	263	2
4	128	192	10.1	0.66	0.0515	0.0022	0.2969	0.0119	0.0416	0.0005	262	71	264	9	263	3
5	90.2	164	8.70	0.55	0.0528	0.0020	0.3044	0.0124	0.0417	0.0005	320	71	270	10	263	3
6	58.6	142	7.25	0.41	0.0521	0.0025	0.2978	0.0136	0.0418	0.0006	290	80	265	11	264	3
7	298	578	30.8	0.52	0.0489	0.0011	0.2843	0.0065	0.0421	0.0004	144	38	254	5	266	2
8	189	597	29.3	0.32	0.0534	0.0012	0.2994	0.0067	0.0416	0.0004	345	35	266	5	262	2
9	62.4	180	9.04	0.35	0.0523	0.0019	0.2956	0.0108	0.0412	0.0005	300	63	263	8	260	3
10	57.0	156	7.84	0.37	0.0527	0.0022	0.3004	0.0130	0.0413	0.0005	314	76	267	10	261	3
11	69.3	189	9.73	0.37	0.0502	0.0023	0.2974	0.0128	0.0419	0.0005	205	78	264	10	264	3
12	92.7	285	13.9	0.33	0.0512	0.0019	0.2982	0.0100	0.0416	0.0004	251	59	265	8	263	3
13	122	314	16.0	0.39	0.0513	0.0017	0.2993	0.0099	0.0419	0.0005	254	56	266	8	265	3
14	148	288	15.1	0.51	0.0539	0.0017	0.3005	0.0096	0.0420	0.0004	367	55	267	8	265	2
15	85.7	203	10.7	0.42	0.0505	0.0020	0.2981	0.0113	0.0419	0.0005	216	66	265	9	264	3
16	188	342	18.2	0.55	0.0523	0.0016	0.3005	0.0093	0.0417	0.0005	296	50	267	7	263	3
17	76.1	166	8.81	0.46	0.0550	0.0026	0.3078	0.0144	0.0420	0.0005	414	84	272	11	265	3
18	48.0	119	6.15	0.40	0.0522	0.0023	0.2979	0.0128	0.0420	0.0006	293	73	265	10	265	4
19	114	223	11.5	0.51	0.0587	0.0020	0.3009	0.0112	0.0416	0.0004	557	64	267	9	263	3
20	123	366	18.5	0.34	0.0547	0.0016	0.3044	0.0094	0.0415	0.0004	398	51	270	7	262	3
21	116	328	16.4	0.35	0.0524	0.0017	0.2977	0.0098	0.0412	0.0004	302	59	265	8	260	2
22	243	684	33.0	0.36	0.0533	0.0010	0.3072	0.0064	0.0416	0.0004	343	30	272	5	263	2
23	61.7	169	8.43	0.37	0.0535	0.0021	0.3008	0.0115	0.0412	0.0005	351	65	267	9	260	3
24	104	230	11.8	0.45	0.0525	0.0019	0.3001	0.0111	0.0415	0.0005	308	63	266	9	262	3
25	163	378	19.4	0.43	0.0517	0.0016	0.2986	0.0085	0.0416	0.0005	271	43	265	7	263	3
26	193	310	16.7	0.62	0.0543	0.0015	0.3003	0.0080	0.0415	0.0004	385	44	267	6	262	2
SMZM-01	Isotopic ratios										Age (Ma)					
Spot	Th (ppm)	U (ppm)	Pb (ppm)	Th/U	$^{207}Pb/^{206}Pb$	1 s	$^{207}Pb/^{235}U$	1 s	$^{206}Pb/^{238}U$	1 s	$^{207}Pb/^{206}Pb$	1 s	$^{207}Pb/^{235}U$	1 s	$^{206}Pb/^{238}U$	1 s
1	84.3	297	15.1	0.28	0.0521	0.0020	0.2994	0.0114	0.0418	0.0005	290	66	266	9	264	3
2	57.1	167	8.51	0.34	0.0526	0.0024	0.2961	0.0134	0.0410	0.0005	313	80	263	10	259	3
3	54.1	153	8.03	0.35	0.0509	0.0034	0.2941	0.0193	0.0426	0.0007	235	119	262	15	269	4
4	53.0	165	8.31	0.32	0.0544	0.0028	0.3024	0.0154	0.0410	0.0006	386	89	268	12	259	4
5	81.8	197	10.4	0.41	0.0517	0.0024	0.2973	0.0129	0.0421	0.0006	274	74	264	10	266	4
6	184	279	15.2	0.66	0.0524	0.0025	0.2934	0.0132	0.0407	0.0006	301	77	261	10	257	3
7	62.7	179	9.08	0.35	0.0534	0.0027	0.3001	0.0145	0.0412	0.0005	346	87	266	11	260	3
8	86.0	296	15.1	0.29	0.0507	0.0020	0.2944	0.0119	0.0420	0.0007	227	62	262	9	265	4
9	61.7	185	9.52	0.33	0.0505	0.0026	0.2883	0.0143	0.0418	0.0005	216	92	257	11	264	3
10	56.5	167	8.43	0.34	0.0528	0.0030	0.2955	0.0157	0.0409	0.0005	320	98	263	12	258	3
11	92.9	288	14.8	0.32	0.0511	0.0024	0.2966	0.0141	0.0419	0.0005	247	86	264	11	264	3
12	54.2	156	7.96	0.35	0.0525	0.0028	0.2948	0.0149	0.0414	0.0005	305	94	262	12	261	3
13	156	277	14.9	0.56	0.0498	0.0024	0.2871	0.0137	0.0417	0.0005	185	90	256	11	263	3
14	66.0	195	9.70	0.34	0.0523	0.0018	0.2965	0.0103	0.0411	0.0004	300	59	264	8	260	3
15	80.6	159	8.24	0.51	0.0529	0.0029	0.2913	0.0155	0.0400	0.0004	322	126	260	12	253	3
16	55.7	144	7.29	0.39	0.0516	0.0025	0.2972	0.0149	0.0416	0.0005	269	94	264	12	263	3
17	67.5	187	9.38	0.36	0.0518	0.0021	0.2994	0.0123	0.0422	0.0005	276	73	266	10	267	3
18	159	347	17.7	0.46	0.0528	0.0017	0.2997	0.0091	0.0412	0.0004	319	54	266	7	260	2
19	57.8	157	8.11	0.37	0.0504	0.0024	0.2943	0.0138	0.0427	0.0005	213	86	262	11	270	3
20	175	265	14.5	0.66	0.0519	0.0020	0.2966	0.0110	0.0416	0.0004	282	66	264	9	263	3
21	50.3	135	6.96	0.37	0.0518	0.0032	0.2962	0.0179	0.0422	0.0006	277	111	263	14	266	4
22	94.3	243	12.4	0.39	0.0510	0.0018	0.2922	0.0103	0.0417	0.0004	240	66	260	8	263	2

Errors are 1σ; Common Pb was corrected using the method proposed by Andersen (2002).

(3.0–5.0 mm, 18–20%), minor orthopyroxene lamellae (2.5–5.5 mm, 2–3%) occurring along prismatic cleavage planes, and K-feldspar (2.5–5.0 mm, 2–3%), in a matrix (60–65%) of clinopyroxene (0.05–0.1 mm, 18–19%), orthopyroxene (0.05–0.1 mm, 5–6%), plagioclase (0.03 ~ 0.05 mm, 26–27%), K-feldspar (0.02–0.05 mm, 5–6%), minor biotite (0.04–0.06 mm, 2–3%), and Ti–Fe oxides (e.g., magnetite) (0.03–0.05 mm, 3–4%).

3. Analytical methods

3.1. Zircon LA-ICP-MS U–Pb dating

Zircon was separated, respectively, from one sample of granodiorite (SMZG-01) and one of gabbro (SMZM-01) using conventional heavy liquid and magnetic techniques at the Langfang Regional Geological Survey, Hebei Province, China. Representative grains were hand-picked under a binocular microscope, mounted in an epoxy resin disc, and then polished and coated with gold film. Zircons were documented with transmitted and reflected light as well as cathodoluminescence imagery to reveal their external and internal structures at the State Key Laboratory of Continental Dynamics, Northwest University, China. Laser ablation techniques were used for zircon age determinations (Table 1). The analyses were completed with an Agilent 7500a ICP-MS, equipped with 193 nm excimer lasers, housed at the State Key Laboratory of Geological Processes and Mineral Resources, China University of Geoscience in Wuhan, China. Zircon 91500 was used as a standard and NIST 610 was used to optimise the results. Spot diameter was 24 μm. Analytical methodology is described in detail in Yuan et al. (2004). Common-Pb corrections were made using the method of Andersen (2002). Data were processed using the GLITTER and ISOPLOT (Ludwig, 2003) programs. Errors on individual analyses by LA-ICP-MS are quoted at the 95% (1σ) confidence level.

3.2. Major and trace elemental analyses

Sixteen granitic samples and fourteen samples of gabbro were selected to carry out major and trace element determinations and Sr–Nd isotopic analysis. Whole-rock samples were trimmed to remove altered surfaces, and were cleaned with deionized water, crushed and powdered with an agate mill.

Major elements were analysed with a PANanalytical Axios-advance (Axios PW4400) X-ray fluorescence spectrometer (XRF) at the State Key Laboratory of Ore Deposit Geochemistry, Institute of Geochemistry, Chinese Academy of Sciences (IGCAS). Fused glass discs were used and the analytical precision, as determined on the Chinese National standard GSR-1 and GSR-3, was better than 5% (Table 2). Loss on ignition (LOI in Table 2) was obtained using 1 g of powder heated at 1100 ºC for 1 h.

Trace element concentrations were determined with an ELAN 6000 ICP-MS at the Institute of Geochemistry, Chinese Academy of Sciences, following procedures described by Qi et al. (2000). The discrepancy between triplicate analyses is less than 5 % for all elements. Analyses of international standards OU-6 and GBPG-1 are in agreement with recommended values (Table 3).

3.3. Sr–Nd isotopic analyses

For Rb–Sr and Sm–Nd isotopic analysis, sample powders were spiked with mixed isotope tracers, dissolved in Teflon capsules with $HF + HNO_3$

Table 2
Major oxides (wt.%) of the studied granodiorites and gabbros.

Sample no.	Rock-type	SiO_2	TiO_2	Al_2O_3	Fe_2O_3	MgO	CaO	Na_2O	K_2O	MnO	P_2O_5	LOI	Total	Mg#	T_{Zr} (°C)
SMZG-01	Granodiorite	58.37	1.25	16.30	8.41	2.08	4.72	5.94	2.27	0.18	0.29	0.87	100.67	33	817
SMZG-03	Granodiorite	60.09	1.32	16.52	8.65	1.89	4.81	3.68	2.60	0.17	0.30	0.77	100.80	30	835
SMZG-07	Granodiorite	60.99	1.14	16.02	7.65	1.63	4.23	3.85	2.68	0.16	0.27	0.95	99.57	30	821
SMZG-08	Granodiorite	60.49	1.23	16.11	8.89	1.78	4.56	3.50	2.56	0.19	0.28	0.64	100.22	29	836
SMZG-10	Granodiorite	59.68	1.26	16.39	8.40	2.06	4.70	4.44	2.23	0.16	0.29	0.78	100.40	33	831
SMZG-11	Granodiorite	58.56	1.31	16.44	9.10	2.16	5.22	3.52	2.30	0.17	0.28	0.82	99.89	32	814
SMZG-12	Granodiorite	60.09	1.24	16.21	8.77	2.04	4.94	3.69	2.55	0.18	0.28	0.73	100.72	32	825
SMZG-13	Granodiorite	59.83	1.26	16.23	8.78	2.12	5.08	3.91	2.16	0.16	0.27	0.89	100.69	33	826
SMZG-15	Granodiorite	59.98	1.20	16.19	8.65	1.97	4.81	3.56	2.38	0.17	0.26	0.76	99.94	31	823
SMZG-16	Granodiorite	58.54	1.32	16.47	9.16	2.20	5.21	3.71	2.34	0.16	0.29	0.78	100.18	32	831
SMZG-17	Granodiorite	59.44	1.27	16.38	8.83	2.11	4.95	3.62	2.41	0.16	0.28	0.76	100.22	32	833
SMZG-18	Granodiorite	59.39	1.16	16.25	8.53	2.19	5.10	3.87	1.79	0.17	0.23	0.88	99.56	34	808
SMZG-19	Granodiorite	59.08	1.30	16.28	9.01	2.13	5.12	3.98	2.37	0.17	0.28	0.86	100.58	32	817
SMZG-21	Granodiorite	59.44	1.20	16.26	9.09	1.98	4.83	3.20	3.25	0.16	0.36	0.92	100.69	30	842
SMZG-24	Granodiorite	58.47	1.16	16.08	8.54	2.17	5.00	5.11	1.99	0.16	0.24	1.11	100.04	34	805
SMZG-28	Granodiorite	59.35	1.17	16.36	8.75	2.18	5.14	3.90	2.22	0.17	0.25	1.1	100.61	33	805
SMZM-01	Gabbro	53.41	1.41	16.64	11.29	3.39	6.81	2.61	1.95	0.18	0.21	1.90	99.81	38	
SMZM-02	Gabbro	52.58	1.48	18.04	11.27	3.08	7.79	2.80	1.78	0.19	0.37	1.19	100.57	35	
SMZM-05	Gabbro	52.23	1.44	17.79	11.29	3.24	7.54	2.68	1.69	0.19	0.32	1.43	99.83	36	
SMZM-06	Gabbro	53.38	1.35	17.64	10.57	3.17	7.51	2.60	1.99	0.18	0.29	2.19	100.87	37	
SMZM-08	Gabbro	54.61	1.29	16.17	11.67	3.67	6.32	2.15	2.01	0.18	0.24	1.32	99.63	39	
SMZM-09	Gabbro	53.45	1.38	16.85	11.17	3.36	6.77	2.80	1.97	0.16	0.20	1.90	100.02	38	
SMZM-10	Gabbro	52.13	1.13	17.75	10.85	3.73	7.45	2.72	2.15	0.18	0.15	1.56	99.81	41	
SMZM-11	Gabbro	54.17	1.45	17.06	11.46	3.48	6.91	2.59	1.65	0.18	0.21	1.77	100.93	38	
SMZM-12	Gabbro	52.82	1.30	17.16	11.32	3.44	6.98	2.53	2.16	0.18	0.23	2.26	100.39	38	
SMZM-13	Gabbro	54.24	1.41	17.08	11.42	3.49	6.92	2.64	1.91	0.17	0.22	1.41	100.90	38	
SMZM-15	Gabbro	52.29	1.35	16.07	11.54	3.92	7.27	3.98	1.87	0.19	0.16	1.62	100.27	40	
SMZM-17	Gabbro	51.46	1.44	17.85	11.44	3.35	7.81	3.19	1.60	0.20	0.34	1.26	99.94	37	
SMZM-18	Gabbro	52.56	1.41	18.18	11.06	2.92	7.36	3.17	1.61	0.19	0.36	1.71	100.54	35	
SMZM-20	Gabbro	54.50	1.19	17.15	10.39	3.16	6.66	3.95	1.95	0.18	0.18	1.38	100.68	38	
GSR-3	RV*	44.64	2.37	13.83	13.4	7.77	8.81	3.38	2.32	0.17	0.95	2.24	99.88		
GSR-3	MV*	44.68	2.36	13.98	13.37	7.75	8.82	3.26	2.31	0.17	0.96	2.15	99.81		
GSR-1	RV*	72.83	0.29	13.4	2.14	0.42	1.55	3.13	5.01	0.06	0.09	0.7	99.62		
GSR-1	MV*	72.76	0.29	13.43	2.16	0.43	1.57	3.16	5.02	0.06	0.1	0.71	99.69		

LOI = Loss on Ignition. RV*: recommended values; MV*: measured values; the values for GSR-1 from Govindaraju (1994) and GSR-3 from Wang et al. (2003a),b). $Mg^{\#} = 100^{*}Mg/(Mg + \sum Fe)$ atomic ratio.

Table 3
The trace elements analysis results (ppm) for the studied granodiorites and gabbros.

Sample no.	Sc	V	Cr	Co	Ni	Ga	Rb	Sr	Y	Zr	Nb	Ba	La	Ce	Pr	Nd	Sm	Eu	Gd	Tb	Dy	Ho	Er	Tm	Yb	Lu	Hf	Ta	Pb	Th	U	Eu/Eu*
SMZM-01	27.3	295	31.5	19.3	12.4	19.5	67.2	523	36.2	95.7	10.3	673	32.2	64.8	8.51	35.2	7.88	1.85	7.27	1.18	6.58	1.41	3.81	0.51	3.19	0.45	2.83	0.61	8.6	7.17	1.22	0.75
SMZM-02	22.6	169	11.6	16.3	6.06	18.3	56.3	576	30.8	83.2	10.9	513	27.7	56.4	7.47	30.9	7.02	1.76	6.05	0.97	5.68	1.21	3.22	0.43	2.70	0.39	2.33	0.63	9.01	5.23	0.94	0.83
SMZM-05	24.2	197	15.3	26.7	9.18	20.1	57.5	596	33	120	11.6	543	30.4	62.8	8.24	33.5	7.31	1.84	6.37	1.06	5.9	1.32	3.50	0.47	2.95	0.42	3.36	0.67	12.1	5.07	0.99	0.82
SMZM-06	22.4	261	67.5	25.6	32.5	18.5	80.3	637	22.9	91.3	8.57	629	20.6	43.1	5.71	22.6	4.58	1.26	4.06	0.66	3.75	0.85	2.48	0.32	2.29	0.34	2.93	0.64	18.4	7.39	1.79	0.89
SMZM-08	21.4	90	40.8	25	18.4	19.5	53.4	625	28.9	92.8	8.54	550	32.5	63.1	8.02	31.9	6.57	1.75	6.03	0.99	5.5	1.15	2.94	0.39	2.44	0.35	2.63	0.55	11.8	6.48	1.44	0.85
SMZM-09	20.6	302	23.5	29.9	12.4	19.7	71.3	470	31.2	185	10.2	515	34.9	68.5	8.52	33	6.68	1.44	5.95	0.96	5.5	1.20	3.35	0.46	2.93	0.43	4.69	0.67	11.2	10.80	2.53	0.70
SMZM-10	27.7	305	14.7	27.6	7.74	20.3	74.2	543	33.9	154	11.6	688	28.7	59	7.66	32.5	7.55	1.78	6.65	1.08	6.27	1.35	3.59	0.47	3.00	0.43	3.94	0.63	11.3	6.52	1.33	0.77
SMZM-11	23.7	319	20.6	27.3	11.9	19.6	80.5	479	25.2	65.3	8.47	458	27	53.6	6.67	25.8	5.27	1.41	4.55	0.76	4.29	0.96	2.70	0.37	2.43	0.36	2.33	0.56	11.3	8.63	1.87	0.88
SMZM-12	28.1	331	10.1	27.3	5.74	21.1	61.6	528	36.2	186	11	567	28.5	59.8	8.06	33.6	7.81	1.86	7.11	1.17	6.59	1.45	3.75	0.50	3.28	0.48	4.60	0.62	10.8	7.03	1.58	0.76
SMZM-13	24.7	309	14	27.8	6.63	21.3	76.8	568	34	110	10.3	760	29.8	60.8	7.95	33.2	7.6	1.78	6.54	1.08	5.95	1.34	3.62	0.46	3.04	0.42	3.09	0.53	11.9	6.48	1.29	0.77
SMZM-15	25.1	299	11.7	31.4	6.88	20.1	55	524	25.4	83.4	8.52	414	23.2	50.3	6.58	25.9	5.46	1.43	4.71	0.76	4.33	0.99	2.63	0.38	2.59	0.37	2.56	0.55	12	5.32	1.18	0.86
SMZM-17	22.7	224	19.9	24	8.39	19.4	51.8	613	24.5	69.2	10.8	404	30.9	59.2	7.41	28.9	5.69	1.62	5.00	0.81	4.31	0.95	2.61	0.34	2.24	0.32	2.12	0.61	9.96	4.71	0.92	0.93
SMZM-18	19.2	172	17.6	21.1	9.94	20.8	49.1	638	26.5	117	9.41	475	31.3	61.7	7.57	30.3	6.28	1.83	5.50	0.87	4.79	1.06	2.83	0.39	2.41	0.35	2.90	0.59	11.2	5.20	1.11	0.95
SMZM-20	21.1	252	14.8	24.9	8.54	20.6	68.6	588	26.3	65.1	8.6	504	26.9	54	6.99	27.5	5.83	1.50	5.36	0.83	4.57	1.00	2.70	0.36	2.32	0.33	2.03	0.44	12	5.78	1.10	0.82
SMZG-01	17.2	118	8.66	15.8	5.59	19.6	75.8	440	28.3	212	9.63	523	29.5	63.9	7.21	29	6.11	1.44	5.22	0.89	5.07	1.13	3.07	0.41	2.90	0.42	5.23	0.66	14.9	11.80	3.48	0.78
SMZG-03	17	118	8.15	15.2	4.91	19.5	84.3	414	27.6	206	9.43	706	29.3	63.3	7.09	28.2	6.09	1.38	5.19	0.89	4.99	1.08	3.01	0.41	2.85	0.42	5.01	0.66	15.8	12.00	3.82	0.75
SMZG-07	15.2	99.8	8.81	12.6	6.98	18	82.6	392	25.8	175	9.49	560	25.8	55.6	6.26	25.2	5.43	1.22	4.66	0.79	4.62	1.02	2.76	0.39	2.57	0.39	4.68	0.79	17.9	11.90	4.12	0.74
SMZG-08	17.7	117	9.43	14.7	5.22	19.9	92.6	424	28.9	205	10	585	30.1	65.4	7.2	29	6.21	1.42	5.24	0.92	5.21	1.13	3.11	0.43	2.99	0.45	5.29	0.73	17.8	13.00	4.39	0.76
SMZG-10	16.2	108	11.3	14.5	8.53	18.9	84	398	26.7	208	9.23	441	31.9	67	7.09	28.3	5.81	1.30	4.85	0.86	4.89	1.07	2.92	0.40	2.77	0.39	5.08	0.61	18.1	12.60	4.02	0.75
SMZG-11	19.4	133	5.34	15.4	3.6	19.2	79.3	415	27.5	172	8.81	427	25.4	55.1	6.43	26.4	5.93	1.32	4.90	0.86	4.93	1.10	2.88	0.42	2.81	0.41	4.30	0.64	14.6	9.01	2.79	0.75
SMZG-12	19.4	127	9.36	15.1	4.54	19.6	90.1	427	27.5	191	8.79	622	27.9	60.1	6.69	27.1	5.9	1.39	5.00	0.86	5.02	1.08	3.00	0.41	2.84	0.43	4.86	0.67	16.3	10.40	3.50	0.78
SMZG-13	17.7	124	6.96	14.4	3.8	19.1	86.3	419	27	197	8.52	375	25.5	56.3	6.37	26.1	5.69	1.32	4.65	0.86	4.82	1.07	2.94	0.41	2.79	0.43	5.00	0.63	14.6	10.00	3.47	0.79
SMZG-15	16.8	125	10	14.9	4.59	18	96.2	442	27.4	181	8.7	524	25.9	52.8	6.5	26.5	5.68	1.36	4.76	0.78	4.62	1.02	2.76	0.40	2.79	0.40	4.37	0.64	14.4	9.74	3.74	0.80
SMZG-16	19.5	140	8.45	16.6	4.49	19.2	104	482	29.4	210	9.13	505	30	61	7.5	30	6.44	1.49	5.32	0.91	5.17	1.13	3.03	0.44	2.99	0.42	5.15	0.60	15.6	10.40	3.46	0.78
SMZG-17	18.8	136	6.01	16	4.46	19.3	109	487	29.1	206	9.09	571	28.9	58.6	7.16	29.2	6.38	1.45	5.35	0.89	5.08	1.10	3.10	0.44	3.02	0.42	4.93	0.65	15.6	10.10	3.78	0.76
SMZG-18	17.8	120	9.06	14.3	4.15	17.3	73.6	390	24.3	158	7.49	301	20.8	42.1	5.53	22.8	5.03	1.24	4.27	0.72	4.28	0.92	2.60	0.36	2.45	0.35	3.93	0.56	15.2	7.62	2.63	0.82
SMZG-19	18.2	130	5.03	14.8	4.18	18.6	87	438	28.3	184	9.06	501	25.3	51.8	6.8	27.4	5.97	1.40	4.92	0.87	4.77	1.08	2.95	0.42	2.84	0.42	4.39	0.64	14.6	9.22	3.10	0.79
SMZG-21	15.7	108	7.49	15.9	4.94	18.8	98.4	451	30.9	227	10.4	652	29.5	61.1	7.76	31	6.6	1.51	5.54	0.96	5.39	1.20	3.23	0.46	3.17	0.45	5.48	0.72	17.3	11.60	4.30	0.76
SMZG-24	18.7	122	9.03	14.4	3.92	18.2	74.9	485	26.9	176	8.13	476	24.7	50	6.42	26	5.25	1.40	4.74	0.81	4.52	1.01	2.79	0.41	2.74	0.38	4.29	0.58	15.2	8.95	2.92	0.86
SMZG-28	18.3	117	10.1	11.7	3.76	17.4	84.2	470	26.5	158	7.88	452	24	49.5	6.22	25.2	5.46	1.33	4.60	0.80	4.54	1.02	2.75	0.40	2.72	0.38	3.76	0.56	12.5	8.87	2.64	0.81
OU-6(RV*)	22.1	129	70.8	29.1	39.8	24.3	120	131	27.4	174	14.8	477	33	74.4	7.8	29.0	5.92	1.36	5.27	0.85	4.99	1.01	2.98	0.44	3.00	0.45	4.70	1.06	28.2	11.51	1.96	
OU-6(MV*)	21.5	129	72.7	28.6	38.7	24.1	109	128	26.9	176	14.7	468	31.5	73	7.6	27.8	5.83	1.32	5.24	0.83	4.85	1.04	2.89	0.41	2.97	0.44	4.82	1.02	27.9	10.70	1.95	
GBPG-1(RV*)	13.9	96.5	181	19.5	59.6	18.6	56.2	364	18.0	232	9.93	908	53.0	103	11.5	43.3	6.79	1.79	4.74	0.60	3.26	0.69	2.01	0.30	2.03	0.31	6.07	0.40	14.1	11.23	0.90	
GBPG-1(MV*)	14.3	101	180	20.1	59.7	19.2	55.8	367	18.4	232	10.2	916	55	98.7	11.9	43.1	6.97	1.84	4.75	0.63	3.18	0.71	2.03	0.31	2.10	0.31	5.92	0.39	13.6	11.40	0.87	

RV*: recommended values; MV*: measured values .The values for GBPG-1 from Thompson et al. (2000), and for OU-6 from Potts and Kane (2005).

Table 4
Sr–Nd isotopic ratios for the representative granodiorites and gabbros.

Sample no.	Sm (ppm)	Nd (ppm)	$^{147}Sm/^{144}Nd$	$^{143}Nd/^{144}Nd$	2σ	$(^{143}Nd/^{144}Nd)$	$\varepsilon_{Nd}(t)$	Rb (ppm)	Sr (ppm)	$^{87}Rb/^{86}Sr$	$^{87}Sr/^{86}Sr$	2σ	$(^{87}Sr/^{86}Sr)$	T_{DM1} (Ga)	T_{DM2} (Ga)
SMZM-02	7.02	30.9	0.1373	0.512251	8	0.512015	−5.6	56.3	576	0.2825	0.708372	10	0.707319	1.79	1.48
SMZM-05	7.31	33.5	0.1319	0.512225	7	0.511999	−5.9	57.5	596	0.2788	0.709242	12	0.708203	1.72	1.51
SMZM-08	6.57	31.9	0.1245	0.512234	10	0.512020	−5.5	53.4	625	0.2469	0.708418	12	0.707498	1.56	1.47
SMZM-12	7.81	33.6	0.1405	0.512269	10	0.512028	−5.3	61.6	528	0.3372	0.708524	14	0.707267	1.83	1.46
SMZM-13	7.60	33.2	0.1384	0.512245	8	0.512008	−5.7	76.8	568	0.3908	0.708689	13	0.707233	1.83	1.49
SMZM-20	5.83	27.5	0.1282	0.512251	12	0.512031	−5.3	68.6	588	0.3372	0.709000	9	0.707743	1.60	1.46
SMZG-01	6.11	29.0	0.1274	0.512549	8	0.512330	0.6	75.8	440	0.4979	0.707322	11	0.705459	1.06	0.98
SMZG-03	6.09	28.2	0.1305	0.512545	12	0.512320	0.4	84.3	414	0.5885	0.707426	11	0.705224	1.11	1.00
SMZG-07	5.43	25.2	0.1303	0.512551	6	0.512327	0.5	82.6	392	0.6090	0.702150	10	0.699872	1.09	0.99
SMZG-08	6.21	29.0	0.1294	0.512539	10	0.512316	0.3	92.6	424	0.6312	0.707625	16	0.705263	1.10	1.00
SMZG-12	5.90	27.1	0.1316	0.512558	9	0.512331	0.6	90.1	427	0.6098	0.707541	12	0.705259	1.10	0.98
SMZG-15	5.68	26.5	0.1296	0.512558	10	0.512335	0.7	96.2	442	0.6290	0.707691	13	0.705338	1.07	0.97
SMZG-17	6.38	29.2	0.1321	0.512567	12	0.512340	0.8	109	487	0.6468	0.707622	12	0.705202	1.09	0.97
SMZG-21	6.60	31.0	0.1287	0.512564	9	0.512342	0.8	98.4	451	0.6305	0.707791	10	0.705432	1.05	0.96

Chondrite Uniform Reservoir (CHUR) values ($^{87}Rb/^{86}Sr = 0.0847$, $^{87}Sr/^{86}Sr = 0.7045$, $^{147}Sm/^{144}Nd = 0.1967$ $^{143}Nd/^{144}Nd = 0.512638$) are used for the calculation. $\lambda_{Rb} = 1.42 \times 10^{-11}$ year^{-1} (Steiger and Jäger, 1977); $\lambda_{Sm} = 6.54 \times 10^{-12}$ year^{-1} (Lugmair and Harti, 1978).

acids, and separated by conventional cation-exchange techniques. Isotopic measurements were performed on a Finnigan MAT-261 thermal ionization mass spectrometer (TIMS) at the State Key Laboratory of Geological Processes and Mineral Resources, China University of Geosciences, China. Procedural blanks were <200 pg for Sm and Nd and <500 pg for Rb and Sr. The mass fractionation corrections for Sr and Nd isotopic ratios were based on $^{86}Sr/^{88}Sr = 0.1194$ and $^{146}Nd/^{144}Nd = 0.7219$, respectively. Analyses of standards during the period of analysis are as follows: NBS987 gave $^{87}Sr/^{86}Sr = 0.710248 \pm 12$ (2σ, $n = 10$); La Jolla gave $^{143}Nd/^{144}Nd = 0.511856 \pm 10$ (2σ, $n = 10$). Our analytical results for Sr–Nd isotopes are presented in Table 4.

3.4. In situ zircon Hf isotopic analysis

In situ zircon Hf isotopic analyses were conducted using a Neptune MC-ICP-MS, equipped with a 193 nm laser, at the Institute of Geology and Geophysics, Chinese Academy of Sciences in Beijing, China. During the analysis, a laser repetition rate of 10 Hz at 100 mJ was used as were spot sizes of 32 and 63 μm. Details of the analytical technique used are described in Xu et al. (2004) and Wu et al. (2006). During the analysis, the $^{176}Hf/^{177}Hf$ and $^{176}Lu/^{177}Hf$ ratios of the standard zircon (91500) were 0.282300 ± 15 ($2\sigma_n$, $n = 24$) and 0.00030, similar to the commonly accepted $^{176}Hf/^{177}Hf$ ratio of 0.282302 ± 8 and 0.282306 ± 8 (2σ) measured using the solution method (Goolaerts et al., 2004; Woodhead et al., 2004). The analytical results are listed in Table 5.

4. Results

4.1. Zircon cathodoluminescence images and U–Pb data

Zircon is relatively abundant in both the granodiorite (SMZG-01) and gabbro (SMZM-01) samples. Prior to LA-ICP-MS zircon U–Pb dating, the surfaces of the grain mounts were washed in dilute HNO_3 and pure alcohol to remove any potential lead contamination. Zircons selected from samples SMZG-01 and SMZM-01 are euhedral, colourless and transparent, mostly elongate-prismatic, and ranged up to 100 μm in diameter. The majority exhibit oscillatory or planar zoning under cathodoluminescence (CL), a typical feature of magmatic zircon. Selected zircon CL images are given in Fig. 2. The studied zircons have variable abundances of Th (54–298 ppm) and U (119–684 ppm), with Th/U ratios of 0.3–0.7 (Table 1), also suggestive of a magmatic origin. On the basis of CL imagery and Th/U ratios, an igneous origin for the zircon is evident. The U–Pb zircon data are presented in Table 1. Analyses of zircon grains with oscillatory structures were concordant and yielded a weighted mean $^{206}Pb/^{238}U$ age of 262.8 ± 1.0 Ma ($n = 26$) for SMZG-01 and 262.1 ± 0.7 Ma ($n = 22$) for SMZM-01 (Fig. 2). The two ages are interpreted as the crystallisation ages of the granodiorite and gabbro.

4.2. Major and trace elements

Major element concentrations of the studied granitic intrusion and gabbro samples are listed in Table 2. These rocks span a wide range of SiO_2 content (51.5–61.0 wt.%), and with the exception of two samples (SMZG-01 and SMZM-15) define a subalkaline suite in the total alkali–silica (TAS) diagram (Fig. 3). The granodiorite samples have relatively high contents of SiO_2 (58.4–61.0 wt.%), Na_2O (3.20–5.94 wt.%) and K_2O (1.79–3.25 wt.%), low MgO (1.63–2.2 wt.%) contents and Mg# values (29–34), and a similar TiO_2 range (1.14–1.32 wt.%). The gabbro samples, in contrast, show a narrow compositional range in SiO_2 (51.5–54.6 wt.%) and are characterised by high Al_2O_3 (16.0–18.2 wt.%) and Na_2O (2.15–3.98 wt.%), low MgO (2.92–3.92 wt.%) and TiO_2 (1.13–1.48 wt.%) contents, as well low Mg# values (35–41). Harker diagrams (Fig. 4) show the variation in major elements as a function of SiO_2-content in both the mafic and granitic rocks. With increasing silica content, TiO_2, Al_2O_3, Fe_2O_{3T}, MgO, CaO and Na_2O decrease, while K_2O increases. P_2O_5 displays a different trend for granitic and mafic rocks with increasing of silica; i.e., there is negative correlation for the gabbro, while no Correlation is evident in the granodiorite (Fig. 4h). Trace element concentrations of the granodiorite and gabbro are listed in Table 3. Selected elements are plotted against SiO_2 content in Fig. 5. Rubidium, Ba and Zr concentrations increase whereas Sr concentrations decrease with increasing SiO_2. All samples have moderate total rare earth element (REE) contents and the gabbro has a slightly wider range in total REE contents (113–174 ppm vs. 113–160 ppm for the granodiorite). Chondrite-normalised patterns for the granodiorite exhibit moderate enrichment of light REE (LREE; $(La/Yb)_N = 5.7–7.8$) and flat heavy REE (HREE; $(Gd/Yb)_N = 1.4–1.5$). Furthermore, the granitic rocks show weakly negative Eu anomalies (Eu/Eu* = 0.74–0.86, Table 3) (Fig. 6a). The gabbro displays similar REE patterns to the granodiorite (Fig. 6b), though the gabbro have relatively larger variation of $(La/Yb)_N$ (5.9–9.3), $(Gd/Yb)_N$ (1.5–2.0) and Eu/Eu* (0.70–0.95). The mafic intrusion is characterised by relatively higher Ga, Nb, Y, Sr, Ba and Sc contents and lower Rb, Zr, Hf, U, Th and Pb contents than the granodiorites, with the exception of sample SMZM-06 (Table 3). On primitive mantle-normalised multi-element diagrams (Fig. 7), the granodiorite samples exhibit enrichment in Rb, Pb, Th and U and significant depletions in Ba, Nb, Ta, P and Ti (Fig. 7a). The gabbro exhibits similar behaviour but with negative Zr–Hf anomalies and without Ba anomalies (Fig. 7b).

4.3. Sr–Nd isotopes

Strontium and Nd isotopic compositions of the representative samples of gabbro and granodiorite are presented in Table 4. The gabbro has relatively constant initial $^{87}Sr/^{86}Sr$ ratios (0.707 to 0.708), and negative $\varepsilon_{Nd}(t)$ values (−5.9 to −5.3). In contrast, the granodiorite

Table 5
Zircon Hf isotopic compositions of the granodiorites and gabbros from NE China.

SMZG-01	$^{176}Yb/^{177}Hf$	2σ	$^{176}Lu/^{177}Hf$	2σ	$^{176}Hf/^{177}Hf$	2σ	$\varepsilon_{Hf}(t)$	T_{DM1} (Ma)	T_{DM2} (Ma)	$f_{Lu/Hf}$
1	0.016028	0.000049	0.000684	0.000002	0.282526	0.000022	−3.1	1020	1478	−0.98
2	0.026553	0.000404	0.001085	0.000015	0.282523	0.000023	−3.3	1035	1489	−0.97
3	0.017220	0.000148	0.000687	0.000006	0.282684	0.000025	2.5	799	1123	−0.98
4	0.031323	0.001031	0.001257	0.000042	0.282580	0.000024	−1.3	959	1363	−0.96
5	0.022732	0.000138	0.000930	0.000004	0.282581	0.000018	−1.2	950	1358	−0.97
6	0.015521	0.000076	0.000612	0.000004	0.282546	0.000024	−2.3	990	1432	−0.98
7	0.061375	0.001121	0.002052	0.000041	0.282630	0.000030	0.4	908	1260	−0.94
8	0.020525	0.000186	0.000814	0.000007	0.282500	0.000021	−4.0	1059	1536	−0.98
9	0.017474	0.000128	0.000751	0.000003	0.282534	0.000023	−2.8	1010	1460	−0.98
10	0.051832	0.000685	0.002052	0.000019	0.282668	0.000022	1.7	852	1173	−0.94
11	0.038395	0.000445	0.001511	0.000018	0.282595	0.000026	−0.8	944	1332	−0.95
12	0.012308	0.000191	0.000559	0.000009	0.282624	0.000021	0.4	880	1257	−0.98
13	0.021705	0.000485	0.000805	0.000020	0.282638	0.000026	0.9	865	1226	−0.98
14	0.020986	0.000072	0.000687	0.000002	0.282680	0.000024	2.4	805	1132	−0.98
15	0.016138	0.000046	0.000712	0.000002	0.282599	0.000022	−0.5	919	1315	−0.98
16	0.016485	0.000054	0.000737	0.000001	0.282574	0.000023	−1.4	953	1369	−0.98
17	0.021555	0.000106	0.000985	0.000002	0.282585	0.000023	−1.0	945	1349	−0.97
18	0.023304	0.000106	0.001013	0.000001	0.282517	0.000025	−3.4	1041	1501	−0.97
19	0.018674	0.000056	0.000751	0.000004	0.282663	0.000024	1.8	829	1170	−0.98
20	0.024587	0.000790	0.001059	0.000035	0.282538	0.000022	−2.7	1013	1454	−0.97
21	0.023145	0.000267	0.000998	0.000012	0.282545	0.000024	−2.5	1002	1439	−0.97
22	0.035827	0.000192	0.001339	0.000005	0.282629	0.000025	0.5	891	1254	−0.96
23	0.021852	0.000269	0.000988	0.000011	0.282611	0.000022	−0.1	908	1289	−0.97
24	0.020196	0.000078	0.000711	0.000004	0.282673	0.000022	2.1	815	1148	−0.98
25	0.014170	0.000146	0.000630	0.000005	0.282566	0.000024	−1.6	962	1386	−0.98
26	0.011754	0.000085	0.000518	0.000004	0.282603	0.000023	−0.3	908	1302	−0.98
SMZM-01	$^{176}Yb/^{177}Hf$	2σ	$^{176}Lu/^{177}Hf$	2σ	$^{176}Hf/^{177}Hf$	2σ	$\varepsilon_{Hf}(t)$	T_{DM1}(Ma)	T_{DM2}(Ma)	$f_{Lu/Hf}$
1	0.033618	0.000818	0.001278	0.000032	0.282473	0.000025	−5.0	1111	1602	−0.96
2	0.022477	0.000282	0.000803	0.000008	0.282531	0.000025	−2.9	1016	1469	−0.98
3	0.021537	0.000465	0.000768	0.000016	0.282525	0.000023	−3.1	1023	1480	−0.98
4	0.013016	0.000125	0.000503	0.000006	0.282522	0.000022	−3.2	1020	1484	−0.98
5	0.018854	0.000110	0.000690	0.000002	0.282530	0.000027	−2.9	1014	1468	−0.98
6	0.020908	0.000222	0.000752	0.000010	0.282532	0.000024	−2.9	1013	1465	−0.98
7	0.024245	0.000384	0.000776	0.000012	0.282544	0.000024	−2.4	997	1438	−0.98
8	0.019101	0.000061	0.000655	0.000002	0.282518	0.000025	−3.3	1030	1495	−0.98
9	0.021870	0.000159	0.000723	0.000006	0.282482	0.000023	−4.6	1081	1575	−0.98
10	0.019908	0.000306	0.000655	0.000004	0.282542	0.000020	−2.5	996	1441	−0.98
11	0.033328	0.000574	0.001340	0.000015	0.282552	0.000028	−2.3	1001	1427	−0.96
12	0.017855	0.000082	0.000725	0.000001	0.282536	0.000023	−2.7	1007	1456	−0.98
13	0.025570	0.000036	0.000938	0.000003	0.282507	0.000023	−3.8	1053	1523	−0.97
14	0.024461	0.000086	0.000903	0.000001	0.282542	0.000023	−2.5	1002	1443	−0.97
15	0.036832	0.000270	0.001346	0.000007	0.282524	0.000025	−3.3	1040	1489	−0.96
16	0.020271	0.000041	0.000802	0.000001	0.282543	0.000025	−2.5	999	1440	−0.98
17	0.026210	0.000279	0.001053	0.000012	0.282532	0.000024	−2.9	1020	1467	−0.97
18	0.026012	0.000325	0.001019	0.000011	0.282508	0.000027	−3.8	1054	1522	−0.97
19	0.020527	0.000106	0.000800	0.000002	0.282504	0.000022	−3.9	1053	1528	−0.98
20	0.029939	0.000018	0.001107	0.000003	0.282538	0.000023	−2.7	1014	1456	−0.97
21	0.038508	0.000985	0.001399	0.000038	0.282516	0.000024	−3.6	1054	1509	−0.96
22	0.021543	0.000163	0.000836	0.000003	0.282549	0.000023	−2.3	991	1427	−0.97

$\varepsilon_{Hf}(t) = 10{,}000\{[(^{176}Hf/^{177}Hf)_S - (^{176}Lu/^{177}Hf)_S * (e^{\lambda t} - 1)]/[(^{176}Hf/^{177}Hf)_{CHUR,0} - (^{176}Lu/^{177}Hf)_{CHUR} * (e^{\lambda t} - 1)] - 1\}$.
$T_{DM*} = 1/\lambda * \ln\{1 + (^{176}Hf/^{177}Hf)S - (^{176}Hf/^{177}Hf)_{DM}]/[(^{176}Lu/^{177}Hf)_S - (^{176}Lu/^{177}Hf)_{DM}]\}$.
$T^C{}_{DM} = 1/\lambda * \ln\{1 + [(^{176}Hf/^{177}Hf)_{S,t} - (^{176}Hf/^{177}Hf)_{DM,\,t}]/[(^{176}Lu/^{177}Hf)_C - (^{176}Lu/^{177}Hf)_{DM}]\} + t$.
The $^{176}Hf/^{177}Hf$ and $^{176}Lu/^{177}Hf$ ratios of chondrite and depleted mantle at the present are 0.282772 and 0.0332, 0.28325 and 0.0384, respectively (Blichert-Toft and Albare`de 1997; Griffin et al. 2000). $\lambda = 1.867 * 10^{-11} a^{-1}$ (Soderlund et al. 2004). $(^{176}Lu/^{177}Hf)_C = 0.015$, t = crystallisation age of zircon.

has distinctly different isotopic compositions, with lower $(^{87}Sr/^{86}Sr)_i$ (0.700–0.705) and positive $\varepsilon_{Nd}(t)$ values (0.3–0.8). This suggests different source regions for the two rock groups. Furthermore, on the $(^{87}Sr/^{86}Sr)_i$ vs. $\varepsilon_{Nd}(t)$ plot (Fig. 8), granodiorite falls within the field given for Mesozoic granites from NE China (Wu et al., 2000a, 2002, 2003a,b, 2005, 2007a) (Fig. 8).

4.4. Zircon Hf isotopes

Two samples of zircon dated by U–Pb methods were also analysed for their Lu–Hf isotopes on the same domains, and the results are listed in Table 5. Twenty-six spot analyses were obtained for the zircon sample SMZG-01, yielding variable $\varepsilon_{Hf}(t)$ values of between −4.0 and +2.5 (Fig. 9a), with two-stage model ages (T_{DM2}) of 1123–1536 Ma, and giving initial $^{176}Hf/^{177}Hf$ ratios ranging from 0.282500 to 0.282684. Twenty-two spot analyses were made for sample SMZM-01. The determined negative $\varepsilon_{Hf}(t)$ values vary between −5.0 and −2.3 (Fig. 9b), corresponding to T_{DM2} model ages in the range from 1427 Ma to 1602 Ma. This sample (SMZM-01) has initial $^{176}Hf/^{177}Hf$ ratios varying between 0.282473 and 0.282552.

5. Discussion

5.1. Petrogenesis

5.1.1. Source regions

The studied gabbro has lower SiO_2 contents (51.5–54.6 wt.%) than liquids produced from partial melting of any of the crustal rocks present (i.e., granitoid liquids; Rapp et al., 2003) (e.g., Zhang et al., 1995; Kato et al., 1997; Gao et al., 1998a,b), suggesting that they were derived from

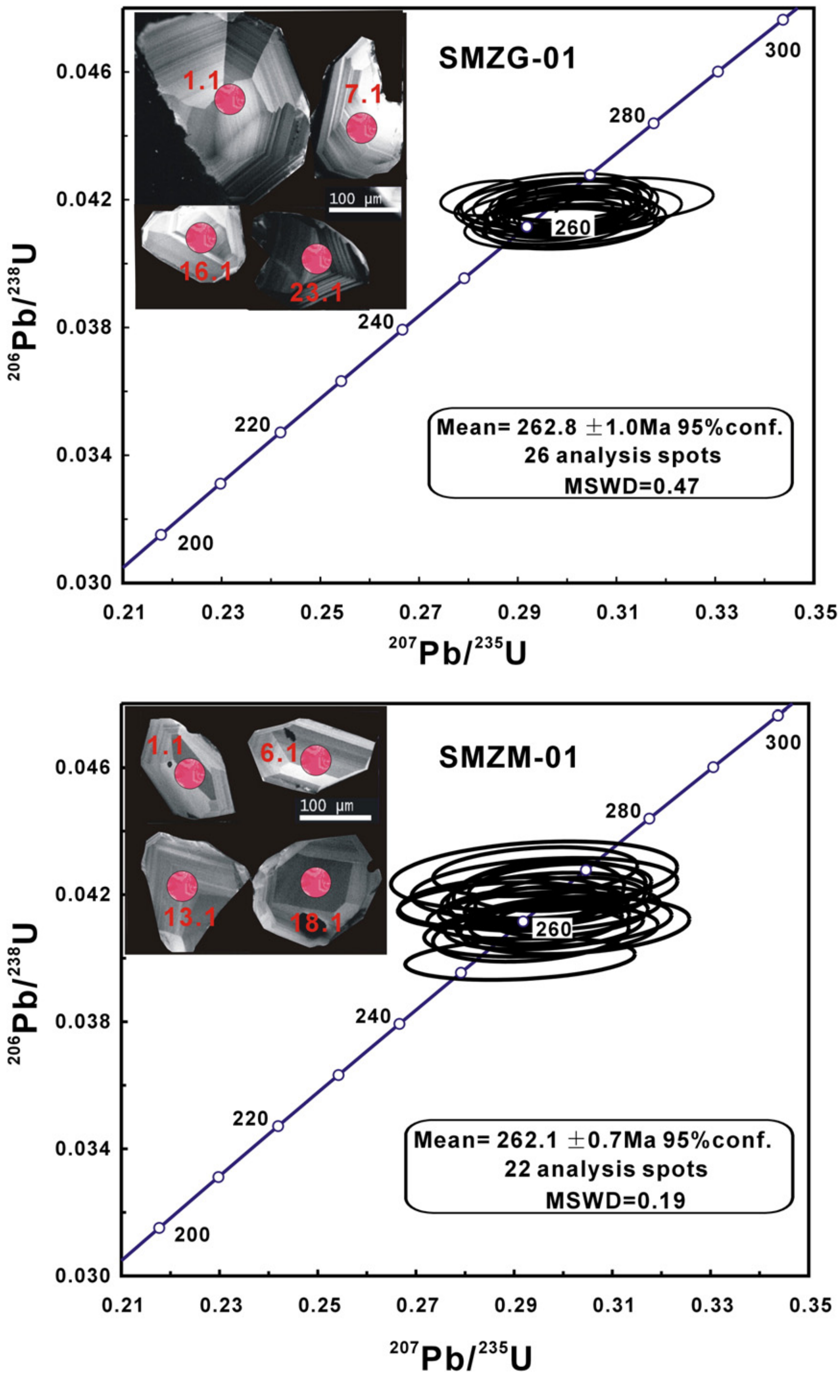

Fig. 2. Representative cathodoluminescence images and LA-ICP-MS U–Pb concordia diagrams for zircon grains from the granitic and mafic samples (SMZG-01 and SMZM-01). The numbers correspond to the spot analyses given in Table 1.

a mantle—rather than a crustal source. The high initial $^{87}Sr/^{86}Sr$ ratios and negative $\varepsilon_{Nd}(t)$ (-5.9 to -5.3) and zircon $\varepsilon_{Hf}(t)$ (-5.0 to -2.3) values (Tables 4 and 5; Figs. 8 and 9b) for the mafic rocks are consistent with derivation from an enriched lithospheric mantle source. By contrast, the granodiorite cannot have been produced by direct melting of mantle peridotite, as these scenarios would not produce melts more silicic than andesite or boninite (~55 wt.% SiO_2) (Baker et al. 1995), which is contrary to observation (58–61 wt.% SiO_2, Table 2). The granodiorites are characterised by low $(^{87}Sr/^{86}Sr)_i$ (0.700–0.705) and slightly positive $\varepsilon_{Nd}(t)$ values (0.3–0.8) (Table 4; Fig. 8), suggesting that they were derived from a source with a slightly depleted mantle characteristic. In addition, recent studies have shown that hafnium isotopic compositions of zircon can elucidate the nature of magma source(s) and the role of magma mixing processes in the generation of granitoid rocks (Griffin et al. 2002; Wang et al., 2003a,b; Kemp and Hawkesworth, 2006; Yang et al. 2006). The determined $\varepsilon_{Hf}(t)$ values (-4.0 to 1.7) for granodiorite indicate that both depleted mantle and crustal sources contributed to the origin of these granitoid rocks (Wu et al., 2007b; Yang et al., 2007).

In order to estimate the proportions of mantle-to-crust component, a simple mixing model was employed, and the result of mixing calculation using Sr–Nd isotopic data is presented in Fig. 8. The plot (Fig. 8) shows that the upper crustal component (UCC) has little or no role in the generation of the studied granodiorite; whereas mantle-

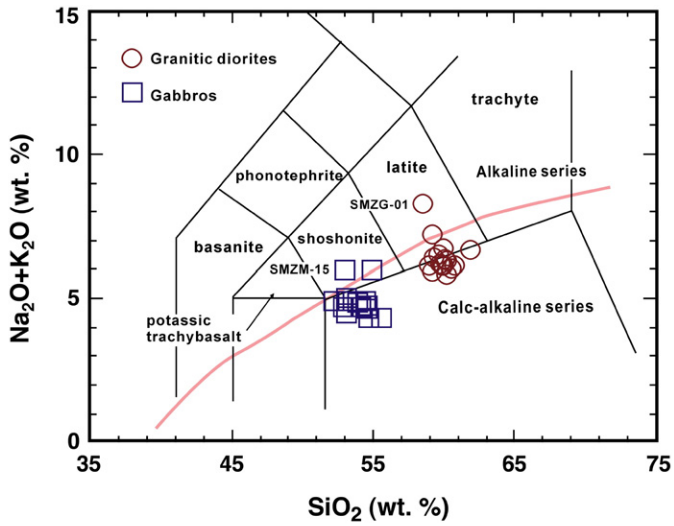

Fig. 3. Total alkali–silica (TAS) diagram for samples of granodiorite and gabbro in this study. All of the major element data have been recalculated to 100 % on a LOI-free basis (after Middlemost, 1994; Le Maitre, 2002).

derived basaltic magma and the lower crust (LCC) are the two major components. While Fig. 8 shows that the mantle component represents about 70–80%, this by no means indicates that the granodiorites were formed by mixing basaltic and lower crustal melts in such proportions. Rather, it suggests that the granitic magmas were produced by melting of a mixed lithology containing lower crustal material (e.g., gneiss, Wu et al., 2003b) that was intruded, or underplated, by a basaltic magma in such proportions (i.e., 70–80% for the latter).

5.1.2. Crustal assimilation

Both the gabbro and granodiorite display positive Pb and negative Ti anomalies in multi-element normalised spider diagrams (Fig. 7), suggesting that continental material could have played a role in the magma genesis of these rocks. This is further supported in much lower Ta/La ratios (0.02–0.03) than primitive mantle (i.e., Ta/La = 0.06: Wood et al. 1979). Crustal contamination might cause significant depletion in Nb–Ta and highly enriched Sr–Nd isotopic signatures in basaltic rocks (Guo et al., 2004b). The gabbro is characterised by negative Nb–Ta anomalies, high and constant initial $^{87}Sr/^{86}Sr$ ratios and negative $\varepsilon_{Nd}(t)$ values (Table 4; Fig. 8), implying that crustal contamination might be significant in these rocks. However, crustal assimilation would induce, to a certain extent, variation in Sr–Nd isotopes, and also results in a positive correlation between Nd, MgO and $\varepsilon_{Nd}(t)$ values, and a negative correlation between MgO and $(^{87}Sr/^{86}Sr)_i$ ratios. These features, however, are not observed in the studied gabbro (not shown), which rules out significant assimilation–fractional crystallisation (AFC) processes during the late evolution of this mafic magma. Similarly, the granodiorite has low initial $^{87}Sr/^{86}Sr$ ratios (0.700–0.705), positive $\varepsilon_{Nd}(t)$ values (0.3–0.8) (Table 4; Fig. 8) and variable zircon $\varepsilon_{Hf}(t)$ values ranging from −4.0 to +1.7 (Table 5; Fig. 9a), suggesting that crustal contamination was also insignificant. In summary, the geochemical (e.g., positive Pb) and Sr–Nd–Hf isotopic signatures of the granitic and mafic rocks appear mainly to have been inherited from their sources (i.e., mixed crustal and enriched mantle sources).

5.1.3. Fractional crystallisation

The gabbro crystallized from a highly fractionated mafic magma as evidenced by low MgO (2.92–3.92 wt.%), Mg# (35–41) (Table 2) and compatible elements, such as Cr (10–68 ppm), Co (16–31 ppm) and Ni (5.7–33 ppm) contents (Table 3). Moreover, there exist negative correlations between SiO_2 and TiO_2, Al_2O_3, Fe_2O_{3T}, MgO, CaO, Na_2O, P_2O_5 (Fig. 4a–f, h), Sr and Zr (Fig. 5b, d), suggesting olivine, clinopyroxene, hornblende, plagioclase, Ti-bearing phases (rutile, ilmenite, titanite, etc.), apatite and zircon fractionation. The separation of plagioclase, Ti–Fe oxides and apatite might account for the observed negative Eu, Nb, Ta, Ti and P anomalies in chondrite-normalised REE patterns and primitive mantle-normalised trace element diagrams (Figs. 6b, 7b). The gabbro, however, was derived from partial melting of a mafic mantle source without plagioclase as a residue (Wu et al., 2005), excluding the possibility of fractionation of plagioclase in the parental magma.

The studied granodiorite samples also have SiO_2 varying negatively with TiO_2, Al_2O_3, Fe_2O_{3T}, MgO, CaO, Na_2O, P_2O_5 (Fig. 4a–f, h), Sr and Zr (Fig. 5b, d), trends which are considered to be related to fractionation of clinopyroxene, hornblende, plagioclase, Ti-bearing phases (rutile, ilmenite, titanite, etc.), apatite and zircon. Additionally, the granodiorite dataset exhibits slightly negative Ba anomalies (Fig. 7a), implying fractionation of K-feldspar. The calculated effects of fractional crystallisation are shown in mineral vector diagrams in Fig. 10a and b. The granodiorite shows a combined vector of K-feldspar and plagioclase fractionation in Fig. 10a and b, however, this also indicates that K-feldspar fractionation was more important than plagioclase in controlling Sr and Ba abundances.

The granodiorite exhibits decreasing Zr with increasing SiO_2 (Fig. 5d) indicating that zircon was saturated in the magma and was also controlled by fractional crystallisation (Li et al., 2007; Zhong et al., 2009). Zircon saturation thermometry (Watson and Harrison, 1983) provides a simple and robust means of estimating felsic magma temperatures from bulk-rock compositions. The calculated zircon saturation temperatures (T_{Zr}°C) of the granitic samples range between 805 and 836 °C (Table 2), which is suggested to be the minimum temperature; the crystallisation temperature of the magma could be higher.

5.1.4. Petrogenetic mechanism

For the genesis of Late Palaeozoic to Mesozoic granites in NE China, four possible tectonic scenarios have been hypothesized (Wu et al., 2003b): (1) a west-dipping subduction zone for the Palaeo-Pacific Ocean; (2) a SE-dipping subduction zone of the Mongolia–Okhotsk Ocean; (3) post-orogenic extensional collapse of the Central Asian orogenic belt; and (4) an anorogenic environment. Generally, granites formed in subduction zones show a roughly linear distribution, which is not the case in those of NE China. Hence, the first two subduction mechanisms are not favoured. Further, although these granites could have formed in an anorogenic setting associated with mantle plume activity, as was suggested by Dobretsov and Vernikovsky (2001), this hypothesis is no longer thought to be a valid explanation due to the large range of emplacement ages and an absence of intense mafic magmatism, often found with anorogenic magmatism (Wu et al., 2003b). In order to account for the huge volumes of granite in NE China, Wu et al. (2003b) proposed that the areal distribution of granites may be related to post-orogenic extensional collapse of the Central Asian Orogenic Belt (CAOB), which is called the Xingmeng (Xing'an-Mongolian) Orogenic belt in the Chinese literature. In other words, granitoid formation was related to massive underplating of mafic magma in an extensional tectonic setting. It is feasible to envisage, therefore, that the studied granodiorite formed in a similar tectonic environment. It has been suggested that the CAOB terminated orogeny during the Late Palaeozoic (~270 Ma), when collapse and crustal extension occurred (Zhao et al., 2008). Further support for an extensional environment for emplacement of the studied granodiorite is provided in the presence of coeval mafic intrusions in the study area. As the crust extended this, in turn, induced upwelling of hot asthenosphere, and it was the high heat flow from this asthenospheric mantle that triggered intense melting in the pre-existing enriched lithospheric mantle resulting in the production of basaltic parental magmas. Subsequent fractionation of the parental magmas resulted in the formation and emplacement of the gabbro under study. Meanwhile, the voluminous

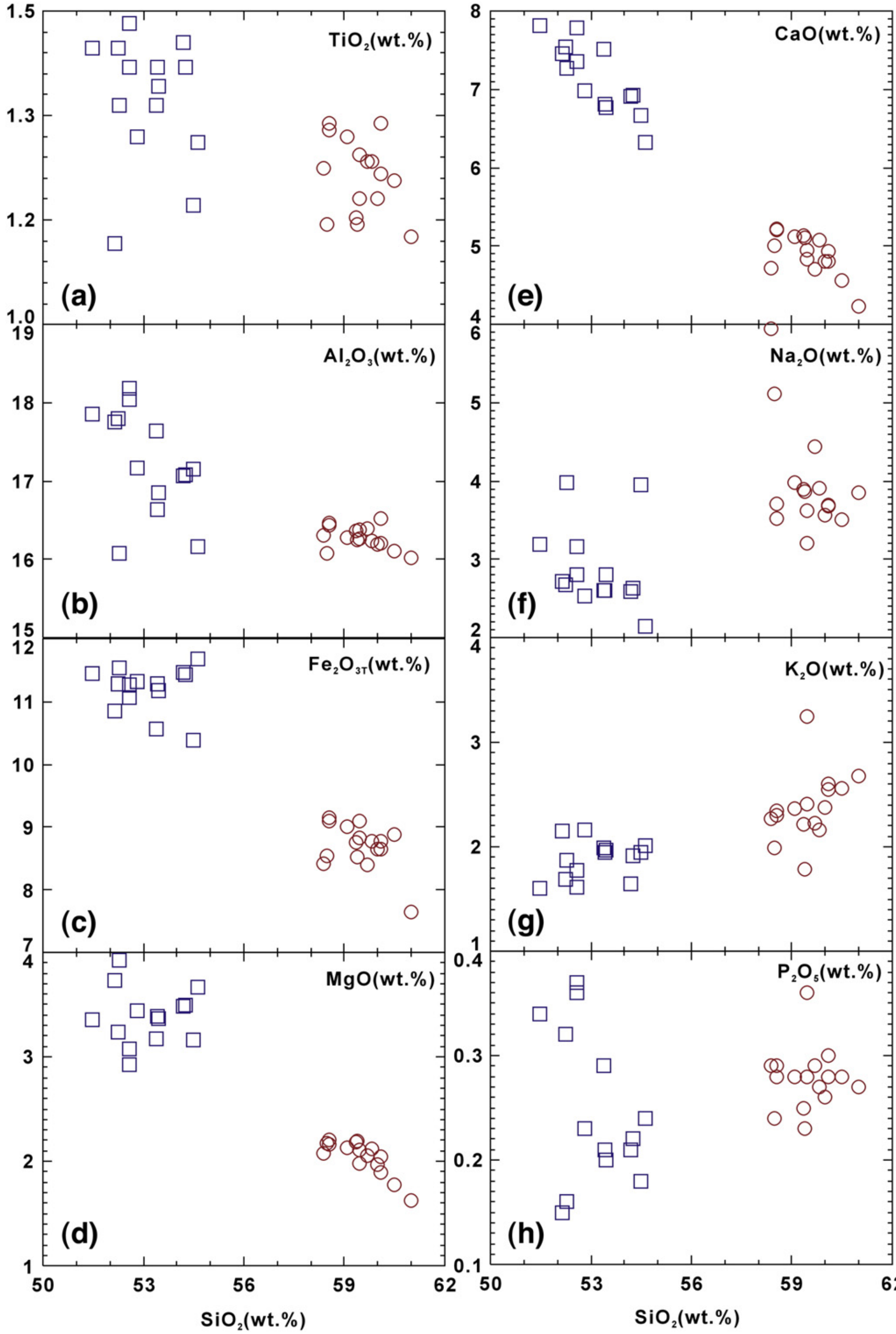

Fig. 4. Chemical variation diagrams (a–h) for major oxides *vs.* SiO_2 content for the granodiorite and gabbro samples in this study. Sample legend as Fig. 3.

granitic magmas were generated by partial melting of pre-existing mixed sources (70–80% juvenile underplated basaltic magma and 20–30% Precambrian lower crust), heated by the upwelling of hot asthenosphere. Thus, we suggest a model in which lithosphere delamination coincided with the granitic and mafic magmatism (Fig. 11).

5.2. Implications for growth of juvenile crust

Granite is the major component of the continental crust on Earth; hence the growth of the continental crust depends much on the mode of generation of granitoid rocks (Wu et al., 2003b). Traditionally, growth of juvenile continental crust is considered to occur at two principal tectonic settings: subduction zones and mantle plumes. The former is most important for the upper continental crust and the latter perhaps, for the lower continental crust (Condie, 1997; cf. the Permian Emeishan large igneous province, SW China, Zhong et al., 2009). The widespread positive range of $\varepsilon_{\mathrm{Nd}}(t)$ from granites present in the CAOB suggests that newly formed mafic lower crust was important in the source region for these Phanerozoic granitoids. Furthermore, several workers have proposed that Phanerozoic crustal growth through

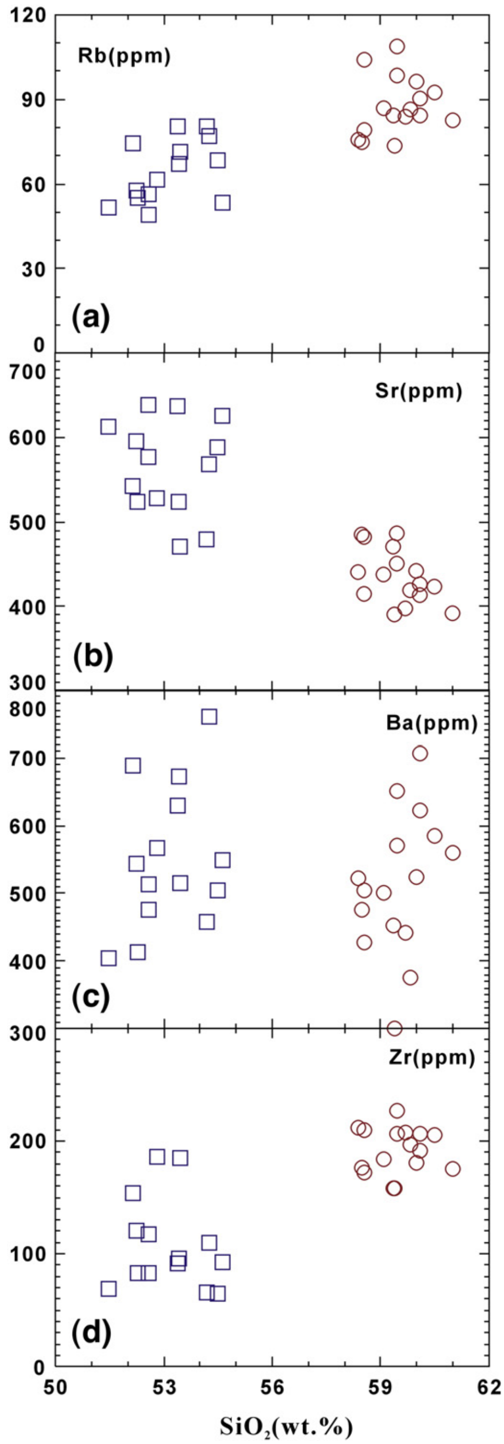

Fig. 5. Variation diagrams (a–d) of selected trace elements *vs.* SiO_2 for the granodiorite and gabbro samples in this study. Sample legend as Fig. 3.

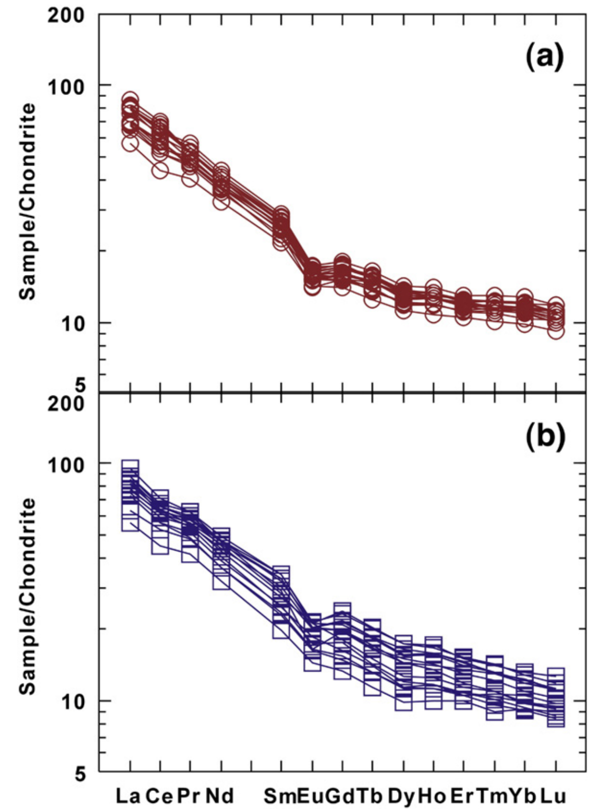

Fig. 6. Chondrite-normalised rare earth element (REE) patterns for the: a) granodiorite and b) gabbro samples in this study. Chondritic REE abundances are after Sun and McDonough (1989).

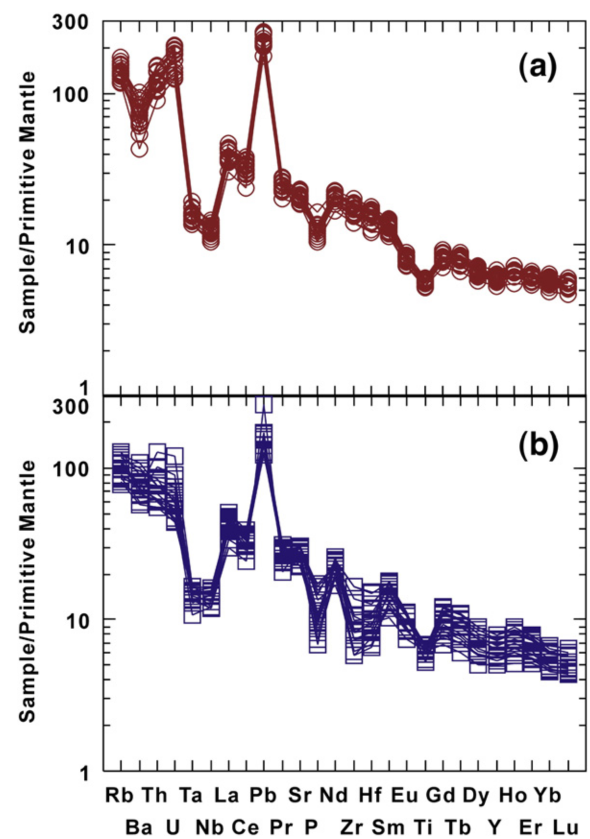

Fig. 7. Primitive mantle-normalised spider diagrams for the: a) granodiorite and b) gabbro samples in this study. Trace element abundances for primitive mantle are after Sun and McDonough (1989).

mantle-derived underplating was significant in the CAOB and that the growth of the continental crust in this region occurred from Meso-Neoproterozoic to the Phanerozoic (e.g., Chen et al., 2000; Wu et al., 2000a, 2002, 2003b; Cheng et al., 2006; Ge et al., 2007). Moreover, the samples from the Jiamusi Block, a Proterozoic microcontinent, have much older model ages of about 1600 Ma (Wu et al., 2000a). However, in the Songliao and Xing'an Blocks, most samples show model ages younger than 1000 Ma, clearly indicating a juvenile nature to the crust in this area. Accordingly, basaltic underplating can also be considered as important in the growth of the continental crust.

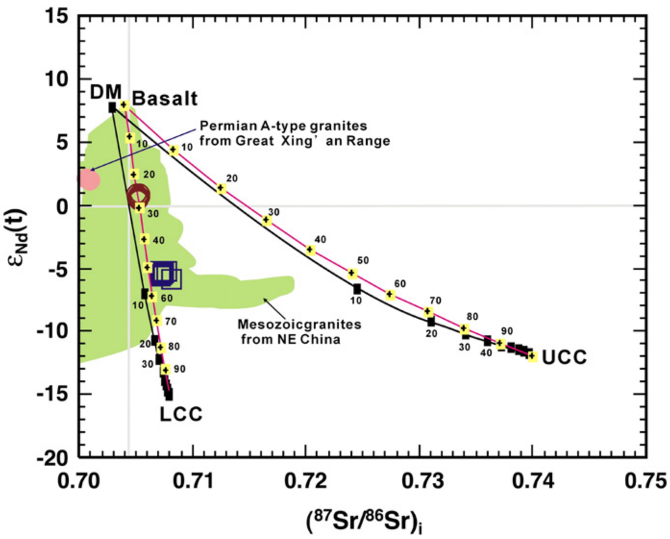

Fig. 8. $\varepsilon_{Nd}(t)$ *vs.* $(^{87}Sr/^{86}Sr)_i$ diagram for granodiorite and gabbro samples in this study from NE China. The numbers indicate the percentages of participation of the crustal materials. Sample legend as Fig. 3. The field for Mesozoic granites in NE China and the Permian A-type granites from Great Xing'an Range, NE China are from Wu et al. (2000a, 2002, 2003a,b, 2005, 2007a). The calculated parameters of Nd (ppm), $\varepsilon_{Nd}(t)$, Sr (ppm) and $(^{87}Sr/^{86}Sr)_i$ are 1.2, +8, 20, and 0.703 from asthenospheric mantle (DM), 15, +8, 200, and 0.704 for basalt; 30, −12, 250, and 0.740 for upper continental crust (UCC); 20, −15, 230, 0.708 for lower continental crust (LCC). All data derive from Wu et al. (2000a).

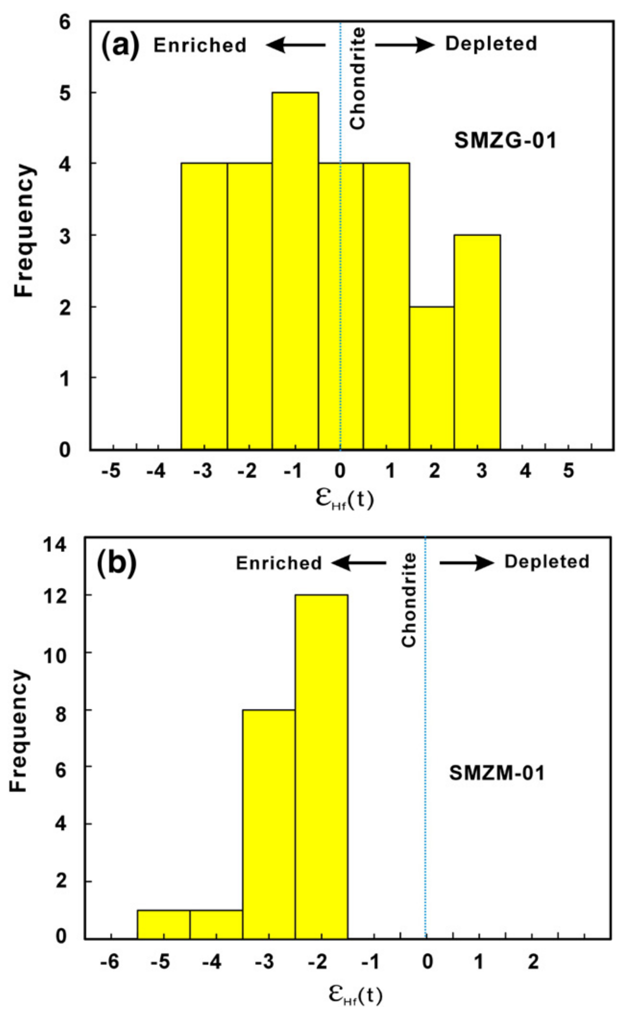

Fig. 9. Histograms of $\varepsilon_{Hf}(t)$ values of zircon with ages of 262.8 Ma in: a) granodiorite (SMZG-01) and b) gabbro (SMZM-01) from the study area, NE China. $\varepsilon_{Hf}(t)$ values for zircon were calculated using the crystallisation ages of the granitic and mafic rocks.

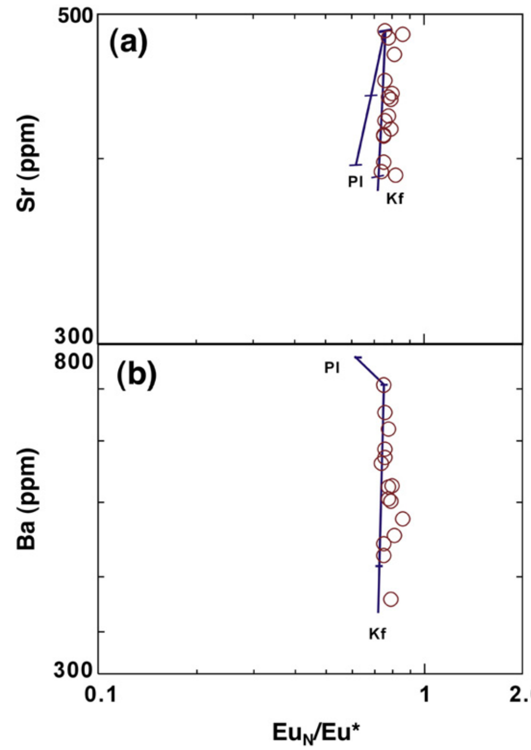

Fig. 10. Plots of Eu/Eu* *vs.*: a) Sr and b) Ba for the granodiorite samples. Mineral fractionation vectors were calculated using partition coefficients from Philpotts and Schnetzler (1970), Schnetzler and Philpotts (1970) and Bacon and Druitt (1988). Tick marks indicate percentage of mineral phase removed in 10% intervals; Pl—plagioclase, Kf—potassium feldspar.

The studied granodiorite samples have positive $\varepsilon_{Nd}(t)$ values with two-stage model ages ranging from 0.96 to 1.0 Ga, and many of the zircons from granodiorite sample SMZG-01 are characterised by positive $\varepsilon_{Hf}(t)$ values of 0.4 to 2.5 with model T_{DM2} ages of between 1123 to 1257 Ma (Table 5). This data could suggest that significant crustal growth by mantle-derived basaltic underplating during Meso-Neoproterozoic times occurred beneath the Songliao Block.

6. Conclusions

Based on the geochronological, geochemical and Sr–Nd–Hf isotopic studies herein, we draw the following conclusions:

(1) LA-ICP-MS U–Pb zircon dating results indicate that the granodiorite intrusion and associated gabbro were intruded at 262.8 ± 1.0 Ma and 262.1 ± 0.7 Ma, respectively. These rocks all formed in a post-orogenic extensional setting.
(2) The granitic rocks and mafic rocks resulted from different sources. The studied granodiorite was probably formed by partial melting of variably mixed sources containing newly underplated basaltic rocks (70–80%) and Precambrian lower crustal material (20–30%). This indicates a significant addition of juvenile crust under NE China during the Meso-Neoproterozoic, which is most characteristic of NE China. Subsequent fractionation of clinopyroxene, hornblende, K-feldspar, plagioclase, Ti-bearing phases (e.g., rutile, ilmenite, titanite), apatite and zircon resulted in the generation and emplacement of granodiorite magmas with negligible crustal contamination. Zircon saturation temperature of between 805 and 836 °C approximately represents the minimum temperature of the granodiorite magma.

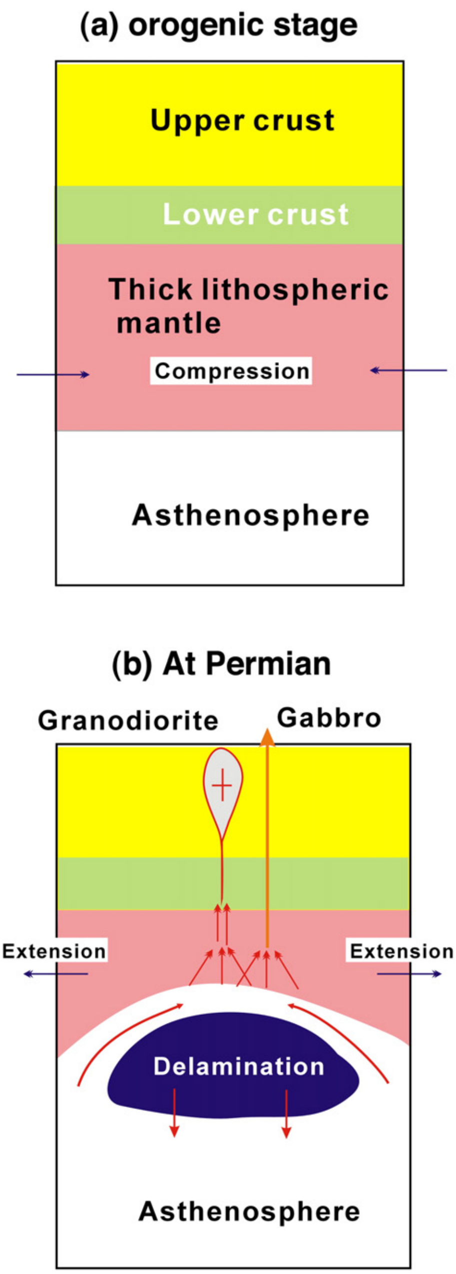

Fig. 11. A petrogenetic–tectonic model for the studied granodiorite and gabbro intrusions. (a) The lithosphere was thickened during the Xingmeng orogenic stage; (b) post-orogenic extensional collapse of orogenic belt, via delamination of the thickened lithospheric mantle, induced upwelling of hot asthenosphere and intense melting of the pre-existing enriched lithospheric mantle and crust (mixed sources), producing parental basaltic and granitic magmas. Subsequently, highly fractionated gabbro and granodiorite were originated by fractional crystallisation.

(3) Gabbro associated with the granodiorite was derived from partial melting of an enriched mantle source related to lithospheric delamination. The parental magma to this also experienced extensive fractionation of olivine, clinopyroxene, hornblende, K-feldspar, Ti-bearing phases (e.g., rutile, ilmenite, titanite), apatite and zircon. Minor, but unimportant, crustal contamination occurred during magma ascent and emplacement.

Acknowledgements

The authors would like to thank Nelson Eby, Qiang Wang and one anonymous reviewer for their constructive reviews on an earlier version of this manuscript. We also thank Ruud Koole for quick editorial handling of the manuscript. This research was supported by the National Nature Science Foundation of China (40673029, 40773020, 90714010, 40634020 and 40521001). We are grateful to Dr. Lian Zhou and Jinhui Yang for help with the Sr, Nd and zircon Hf isotopic analysis, and Yongsheng Liu and Zhao-Chu Hu are thanked for help with LA-ICP-MS zircon U–Pb dating. The authors also thank Hu-jun Gong for helping with CL image handling.

References

Andersen, T., 2002. Correction of common lead in U–Pb analyses that do not report ^{204}Pb. Chemical Geology 192, 59–79.
Bacon, C.R., Druitt, T.H., 1988. Compositional evolution of the zoned calcalkaline magma chamber of Mount-Mazama, Crater Lake, Oregon. Contributions to Mineralogy and Petrology 98, 224–256.
Baker, M.B., Hischmann, M.M., Ghiorso, M.S., Stolper, E.M., 1995. Compositions of near-solidus peridotite melt from experiments and thermodynamic calculations. Nature 375, 308–311.
Blichert-Toft, J., Albare`de, F., 1997. The Lu–Hf geochemistry of chondrites and the evolution of the mantle–crust system. Earth and Planetary Science Letters 148, 243–258.
Chen, B., Jahn, B.M., 2002. Geochemical and isotopic studies of the sedimentary and granitic rocks of the Altai orogen of northwest China and their tectonic implications. Geological Magazine 139, 1–13.
Chen, B., Jahn, B.M., Wilde, S., Xu, B., 2000. Two constrasting Paleozoic magmatic belts in northern Inner Mongolia, China: petrogenesis and tectonic implications. Tectonophysics 328, 157–182.
Cheng, R.Y., Wu, F.Y., Ge, W.C., Sun, D.Y., Liu, X.M., Yang, J.H., 2006. Emplacement age of the Raohe Complex in eastern Heilongjiang Province and the tectonic evolution of the eastern part of Northeastern China. Acta Petrologica Sinica 22 (2), 353–376.
Condie, K.C., 1997. Contrasting sources for upper and lower continental crust: the greenstone connection. Journal of Geology 105, 729–736.
Dobretsov, N.L., Vernikovsky, V.A., 2001. Mantle plumes and their geological manifestations. International Geology Review 43, 771–787.
Gao, S., Luo, T.-C., Zhang, B.-R., Zhang, H.-F., Han, Y.-W., Zhao, Z.-D., Hu, Y.-K., 1998a. Chemical composition of the continental crust as revealed by studies in East China. Geochimica et Cosmochimica Acta 62, 1959–1975.
Gao, S., Zhang, B.-R., Jin, Z.-M., Kern, H., Luo, T.-C., Zhao, Z.-D., 1998b. How mafic is the lower continental crust? Earth and Planetary Science Letters 106, 101–117.
Ge, W.C., Wu, F.Y., Zhou, C.Y., Zhang, J.H., 2005. Zircon U–Pb ages and its significance of the Mesozoic granites in the Wulanhaote region, central Da Hinggan Mountain. Acta Petrologica Sinica 21 (3), 749–762.
Ge, W.C., Sui, Z.M., Wu, F.Y., Zhang, J.H., Xu, X.C., Cheng, R.Y., 2007. Zircon U–Pb ages, Hf isotopic characteristics and their implications of the Early Paleozoic granites in the northeastern Da Hinggan Mts, northeastern China. Acta Petrologica Sinica 23 (2), 423–440.
Goolaerts, A., Mattielli, N., de Jong, J., Weis, D., Scoates, J.S., 2004. Hf and Lu isotopic reference values for the zircon standard 91500 by MC-ICP-MS. Chemical Geology 206, 1–9.
Govindaraju, G., 1994. Compilation of working values and sample description for 383 geostandards. Geostandard Newsletter 18, 1–158.
Griffin, W.L., Pearson, N.J., Belousova, E., Jackson, S.E., van Achterbergh, E., O'Reilly, S.Y., Shee, S.R., 2000. The Hf isotope composition of cratonic mantle: LAM-MC-ICPMS analysis of zircon megacrysts in kimberlites. Geochimica et Cosmochimica Acta 4, 133–147.
Griffin, W.L., Wang, X., Jackson, S.E., Pearson, N.J., O'Reilly, S.Y., 2002. Zircon geochemistry and magma mixing, SE China: in-situ analysis of Hf isotopes, Tonglu and Pingtan igneous complexes. Lithos 61, 237–269.
Guo, C.L., Wu, F.Y., Yang, J.H., Lin, J.Q., Sun, D.Y., 2004a. The extensional setting of the Early Cretaceous magmatism in eastern China: example from the Yinmawanshan pluton in southern Liaodong Peninsula. Acta Petrologica Sinica 20 (5), 1193–1204.
Guo, F., Fan, W.M., Wang, Y.J., Zhang, M., 2004b. Origin of early Cretaceous calc-alkaline lamprophyres from the Sulu orogen in eastern China: implications for enrichment processes beneath continental collisional belt. Lithos 78, 291–305.
HBGMR (Heilongjiang Bureau of Geology and Mineral Resources), 1993. Regional Geology of Heilongjiang Province (in Chinese with English summary). Geological Publishing House, Beijing, pp. 347–438.
IMBGMR (Inner Mongolian Bureau of Geology and Mineral Resources), 1990. Regional Geology of Inner Mongolian Autonomous Region (in Chinese with English summary). Geological Publishing House, Beijing, p. 725.
Jahn, B.M., 2002. Generation of the juvenile crust in the Central Asian Orogenic Belt. In: Wu, F.Y., Wilde, S.A., Jahn, B.M. (Eds.), IGCP-420 4th Workshop Abstracts and Excursion Guidebook, Changchun, China, pp. 57–68.
Jahn, B.M., Wu, F.Y., Chen, B., 2000a. Massive granitoid generation in Central Asia: Nd isotope evidence and implication for continental growth in the Phanerozoic. Episodes 23, 82–92.
Jahn, B.M., Wu, F.Y., Hong, D.W., 2000b. Important crustal growth in the Phanerozoic: isotopic evidence of granitoids from East-central Asia. Proc. Indian Acad. Sci. Earth and Planetary Science Letters 109, 5–20.
JBGMR (Jilin Bureau of Geology and Mineral Resources), 1988. Regional Geology of Jilin Province (in Chinese with English summary). Geological Publishing House, Beijing, pp. 301–385.
Kato, T., Enami, A., Zhai, M., 1997. Ultrahigh-pressure marble and eclogite in the Su–Lu ultrahigh-pressure terrane, eastern China. Journal of Metamorphic Geology 15, 169–182.

Kemp, A.I.S., Hawkesworth, C.J., 2006. Using hafnium and oxygen isotopes in zircons to unravel the record of crustal evolution. Chemical Geology 226, 144–162.
Le Maitre, R.W., 2002. Igneous Rocks: A Classification and Glossary of Terms, (2nd). Cambridge University Press, Cambridge. 236.
Li, X.H., Li, Z.X., Li, W.X., Liu, Y., Yuan, C., Wei, G.J., Qi, C.S., 2007. U–Pb zircon, geochemical and Sr–Nd–Hf isotopic constraints on age and origin of Jurassic I- and A-type granites from central Guangdong, SE China: a major igneous event in response to foundering of a subducted flat-slab? Lithos 96, 186–204.
Ludwig, K.R., 2003. ISOPLOT 3.0: A Geochronological Toolkit for Microsoft Excel, Berkeley Geochronology Center. Special publication no. 4.
Lugmair, G.W., Harti, K., 1978. Lunar initial $^{143}Nd/^{144}Nd$: differential evolution of the lunar crust and mantle. Earth Planetary Science Letters 39, 349–357.
Middlemost, E.A.K., 1994. Naming materials in the magma/igneous rock system. Earth-Science Reviews 74, 193–227.
Philpotts, J.A., Schnetzler, C.C., 1970. Phenocryst–matrix partition coefficients for K, Rb, Sr and Ba, with applications to anorthosite and basalt genesis. Geochimica et Cosmochimica Acta 34, 307–322.
Potts, P.J., Kane, J.S., 2005. International association of geoanalysts certificate of analysis: certified reference material OU-6 (Penrhyn slate). Geostandards and Geoanalytical Research 29, 233–236.
Qi, L., Hu, J., Grégoire, D.C., 2000. Determination of trace elements in granites by inductively coupled plasma mass spectrometry. Talanta 51, 507–513.
Qin, K., 1995. Geological features of magmatic sulfide Cu–Ni deposit at the Hongqiling, Jilin Province. Jilin Geology 3, 17–30 (in Chinese with English abstract).
Rapp, R.P., Shimizu, N., Norman, M.D., 2003. Growth of early continental crust by partial melting of eclogite. Nature 425, 605–609.
Schnetzler, C.C., Philpotts, J.A., 1970. Partition coefficients of rare-earth elements between igneous matrix material and rock-forming mineral phenocrysts; II. Geochimica et Cosmochimica Acta 34, 331–340.
Soderlund, U., Patchett, P.J., Vervoort, J.D., Isachsen, C.E., 2004. The ^{176}Lu decay constant determined by Lu–Hf and U–Pb isotope systematics of Precambrian mafic intrusions. Earth and Planetary Science Letters 219, 311–324.
Steiger, R.H., Jäger, E., 1977. Subcommission on geochronology; convention on the use of decay constants in geochronology and cosmochronology. Earth Planetary Science Letters 36, 359–362.
Sun, S.S., McDonough, W.F., 1989. Chemical and isotopic systematics of oceanic basalts: implications for mantle composition and processes. In: Saunders, A.D., Norry, M.J. (Eds.), Magmatism in the Ocean Basins. Geological Society Special Publication, London, pp. 313–345.
Sun, D.Y., SUZUK, K., Wu, F.Y., Lu, X.P., 2005. CHIME dating and its application for Mesozoic granites of Huanggoushan, Jilin Province. Geochimica 34 (4), 305–314.
Sun, J.G., Men, L.J., Zhao, J.K., Chen, L., Liang, S.N., Chen, D., Pang, W., 2008. Zircon chronology of melanocratic dykes in the district of the Xiaoxinancha Au-rich Cu deposit in Yanbian and its geological implication. Acta Geologica Sinica 82 (4), 517–527 in Chinese with English abstract.
Thompson, M., Potts, P.J., Kane, J.S., Wilson, S., 2000. An international proficiency test for analytical geochemistry laboratories-report on round 5 (August 1999). Geostandards and Geoanlytical Research 24, E1–E28.
Wang, X., Griffin, W.L., Wang, Z., Zhou, X.M., 2003a. Hf isotope compositions of zircons and implications for the petrogenesis of Yajiangqiao granite, Hunan Province, China. Chinese Science Bulletin 48, 995–998.
Wang, Y.M., Gao, Y.S., Han, H.M., Wang, X.H., 2003b. Practical Handbook of Reference Materials for Geoanalysis. Geological publishing House. in Chinese.
Watson, E.B., Harrison, T.M., 1983. Zircon saturation revisited: temperature and composition effects in a variety of crustal magma types. Earth and Planetary Science Letters 64, 295–304.
Wilde, S., Zhang, X.Z., Wu, F.Y., 2000. Extension of a newly identified 500 Ma metamorphic terrain in North East China: further U–Pb SHRIMP dating of the Mashan Complex, Heilongjiang Province, China. Tectonophysics 328, 115–130.
Wood, D.A., Tarneu, J., Varet, J., Saunders, A.N., Bouhault, H., Joron, J.L., Treuil, M., Cann, J.R., 1979. Geochemistry of basalts drills in the North Atlantic by IPOD Leg 49: implications for mantle heterogeneity. Earth Planetary Science Letters 42, 77–97.
Woodhead, J., Hergt, J., Shelley, M., Eggins, S., Kemp, R., 2004. Zircon Hf-isotope analysis with an excimer laser, depth profiling, ablation of complex geometries, and concomitant age estimation. Chemical Geology 209, 121–135.
Wu, F.Y., Jahn, B.M., Wilde, S.A., Sun, D.Y., 2000a. Phanerozoic continental crustal growth: U–Pb and Sr–Nd isotopic evidence from the granites in northeastern China. Tectonophysics 328, 89–113.
Wu, F.Y., Sun, D.Y., Li, H.M., Lin, Q., 2000b. The zircon U–Pb ages of Songliao basement rocks. Chinese Science Bulletin 45, 1514–1518.
Wu, F.Y., Sun, D.Y., Li, H.M., Wang, X.L., 2001. The nature of basement beneath the Songliao Basin in NE China: geochemical and isotopic constraints. Physics and Chemistry of the Earth (part A) 26, 793–803.
Wu, F.Y., Sun, D.Y., Li, H.M., Jahn, B.M., Wilde, S.A., 2002. A-type granites in Northeastern China: age and geochemical constraints on their petrogenesis. Chemical Geology 187, 143–173.
Wu, F.Y., Jahn, B.M., Wilde, S.A., Lo, C.H., Yui, T.F., Lin, Q., Ge, W.C., Sun, D.Y., 2003a. Highly fractionated I-type granites in NE China (I): geochronology and petrogenesis. Lithos 66, 241–273.
Wu, F.Y., Jahn, B.M., Wilde, S.A., Lo, C.H., Yui, T.F., Lin, Q., Ge, W.C., Sun, D.Y., 2003b. Highly fractionated I-type granites in NE China (II): isotopic geochemistry and implications for crustal growth in the Phanerozoic. Lithos 67, 191–204.
Wu, F.Y., Simon, A.W., Zhang, G.L., Sun, D.Y., 2004a. Geochronology and petrogenesis of the post-orogenic Cu–Ni sulfide-bearing mafic–ultramafic complexes in Jilin Province, NE China. Journal of Asian Earth Sciences 23, 781–797.
Wu, F.Y., Sun, D.Y., Jahn, B.M., Wilde, S.A., 2004b. A Jurassic garnet-bearing granitic pluton from NE China showing tetrad REE patterns. Journal of Asian Earth Science 23, 731–744.
Wu, F.Y., Yang, J.H., Wilde, S.A., Zhang, X.O., 2005. Geochronology, petrogenesis and tectonic implications of the Jurassic granites in the Liaodong Penisula, NE China. Chemical Geology 221, 127–156.
Wu, F.Y., Yang, Y.H., Xie, L.W., Yang, J.H., Xu, P., 2006. Hf isotopic compositions of the standard zircons and baddeleyites used in U–Pb geochronology. Chemical Geology 234, 105–126.
Wu, F.Y., Li, X.H., Yang, J.H., Zheng, Y.F., 2007a. Discussions on the petrogenesis of granites. Acta Petrotogica Sinica 23 (6), 1217–1238.
Wu, F.Y., Li, X.H., Zheng, Y.F., Gao, S., 2007b. Lu–Hf isotopic systematics and their applications in petrology. Acta Petrologica Sinica 23, 185–220.
Wu, G., Chen, Y.J., Sun, F.Y., Li, J.C., Li, Z.T., Wang, X.J., 2008. Geochemistry of the Late Jurassic granitoids in the northern end area of Da Hinggan Mountains and their geological and prospecting implications. Acta Petrologica Sinica 24 (4), 899–910.
Xu, P., Wu, F.Y., Xie, L.W., Yang, Y.H., 2004. Hf isotopic compositions of the standard zircons for U–Pb dating. Chinese Science Bulletin 49, 1642–1648.
Yang, J.H., Wu, F.Y., Chung, S.L., Wilde, S.A., Chu, M.F., 2004. Multiple sources for the origin of granites: geochemical and Nd/Sr isotopic evidence from Gudaoling granite and its mafic enclaves, NE China. Geochimica et Cosmochimica Acta 68, 4469–4483.
Yang, J.H., Wu, F.Y., Chung, S.L., Wilde, S.A., Chu, M.F., 2006. A hybrid origin for the Qianshan A-type granite, northeast China: geochemical and Sr–Nd–Hf isotopic evidence. Lithos 89, 89–106.
Yang, J.H., Wu, F.Y., Wilde, S.A., Xie, L.W., Yang, Y.H., Liu, X.M., 2007. Tracing magma mixing in granite genesis: in situ U–Pb dating and Hf-isotope analysis of zircons. Contributions to Mineralogy and Petrology 153, 177–190.
Ye, M., Zhang, S.H., Wu, F.Y., 1994. The classification of the Paleozoic tectonic units in the area crossed by Manzhouli–Suifenghe geoscience transect (in Chinese with English abstract). Journal of Changchun University (Earth Science) 24, 241–245.
Yuan, H.L., Gao, S., Liu, X.M., Li, H.M., Gunther, D., Wu, F.Y., 2004. Accurate U–Pb age and trace element determinations of zircon by laser ablation–inductively coupled plasma mass spectrometry. Geostandards Newsletter 28, 353–370.
Zhang, R.Y., Hirajima, T., Banno, S., Cong, B., Liou, J.G., 1995. Petrology of ultrahigh-pressure metamorphic rocks in southern Sulu region, eastern China. Journal of Metamorphic Geology 13, 659–675.
Zhang, Y.B., Wu, F.Y., Li, H.M., Lu, X.P., Sun, D.Y., Zhou, H.Y., 2002a. Single grain zircon U–Pb ages of the Huangniling granite in Jilin province. Acta Petrologica Sinica 18 (4), 475–481.
Zhang, Y.B., Wu, F.Y., Sun, D.Y., Li, H.M., 2002b. Single grain zircon U–Pb ages of the "Early Hercynian" Miantian granites and Zhongping hypersthene diorite in the Yanbian area. Geological Review 48 (4), 424–429.
Zhang, J.F., Li, Z.T., Jin, C.Z., 2004. Adakites in northeastern China and their mineralized implications. Acta Petrologica Sinica 20 (2), 361–368.
Zhang, X.Z., Yang, B.J., Wu, F.Y., Liu, G.X., 2006. The lithosphere structure in the Hingmong-Jihei (Hinggan–Mongolia–Jilin–Heilongjiang) region, northeastern China. Geology in China 33 (4), 816–823.
Zhao, Z.H., Bai, Z.H., Xiong, X.L., Mei, H.J., Wang, Y.X., 2000. Geochemistry of alkali-rich igneous rocks of northern Xinjiang and its implications for geodynamics. Acta Geologica Sinica 74, 321–328.
Zhao, Q.Y., Li, C.F., Li, D.C., Chen, Y.J., 2008. Dating for zircons from gabbro dike of Wudaogou Group in Yanbian area and its geological significance. Global Geology 27 (2), 150–155 in Chinese with English abstract.
Zhong, H., Zhu, W.G., Hu, R.Z., Xie, L.W., He, D.F., Liu, F., Chu, Z.Y., 2009. Zircon U–Pb age and Sr–Nd–Hf isotope geochemistry of the Panzhihua A-type syenitic intrusion in the Emeishan large igneous province, southwest China and implications for growth of juvenile crust. Lithos 110, 109–128.